OPEN ACCESS

Journal of Statistical Mechanics: Theory and Experiment
An IOP and SISSA journal

PAPER: Quantum statistical physics, condensed matter, integrable systems

Exactly solvable non-unitary time evolution in quantum critical systems I: effect of complex spacetime metrics

Xueda Wen[1,2,3]

[1] School of Physics, Georgia Institute of Technology, Atlanta, GA 30332, United States of America
[2] Department of Physics, Harvard University, Cambridge, MA 02138, United States of America
[3] Department of Physics, University of Colorado, Boulder, CO 80309, United States of America
E-mail: xueda.wen@physics.gatech.edu

Received 31 July 2024
Accepted for publication 10 September 2024
Published 29 October 2024

Online at stacks.iop.org/JSTAT/2024/103103
https://doi.org/10.1088/1742-5468/ad7c3d

Abstract. In this series of works, we study exactly solvable non-unitary time evolutions in one-dimensional quantum critical systems ranging from quantum quenches to time-dependent drivings. In this part I, we are motivated by the recent works of Kontsevich and Segal (2021 arXiv:2105.10161) and Witten (2021 arXiv:2111.06514) on allowable complex spacetime metrics in quantum field theories. In general, such complex spacetime metrics will lead to non-unitary time evolutions. In this work, we study the universal features of such non-unitary time evolutions based on exactly solvable setups. Various physical quantities including the entanglement Hamiltonian and entanglement spectrum, entanglement entropy, and energy density at an arbitrary time can be exactly solved. Due to the damping effect introduced by the complex time, the excitations in the initial state are gradually damped out in time. The non-equilibrium dynamics

exhibit universal features that are qualitatively different from the case of real-time evolutions. For instance, for an infinite system after a global quench, the entanglement entropy of the semi-infinite subsystem will grow logarithmically in time, in contrast to the linear growth in a real-time evolution. Moreover, we study numerically the time-dependent driven quantum critical systems with allowable complex spacetime metrics. It is found that the competition between driving and damping leads to a steady state with an interesting entanglement structure.

Keywords: entanglement entropies,
entanglement in extended quantum systems, quantum criticality,
dissipative systems

Contents

J. Stat. Mech. (2024) 103103

1. Introduction

1.1. Introduction and motivation

Recently in [1], Kontsevich and Segal (KS) studied a class of complex spacetime geometries where a generic quantum field theory can be consistently defined, such that the path integral is manifestly convergent on the allowed geometries. KS's motivation was to develop an alternative to some of the standard axioms of quantum field theories [2] by postulating that the partition function and the correlation functions extend analytically to a certain domain of complex spacetime metrics. They studied the *allowable* metrics g by considering the path integral over matter fields, which are taken to be scalars and p-form fields of all possible ranks with real values. KS give an explicit description of the allowable metrics g. First, one can write the metric in a diagonal form $g_{ij} = \delta_{ij}\lambda_i$ (λ_i are complex numbers in general), which can always be done locally, then by requiring the convergence of the path integral one can obtain

$$\Sigma := \sum_{i=1}^{D} |\mathrm{Arg}\,(\lambda_i)\,| < \pi, \tag{1}$$

where $\mathrm{Arg}(z) \in (-\pi, \pi]$ is the argument of $z \in \mathbb{C}$, and D is the spacetime dimension. Conversely, if the condition in (1) is satisfied, then we say that the metric g is allowable. The condition in (1) generalizes the result in an earlier work by Louko and Sorkin in two dimensions [3] to arbitrary dimensions.

As noted by KS, the space of allowable metrics is contractible onto the space of Euclidean metrics. Note that Euclidean metrics with

$$\mathrm{d}s^2 = \mathrm{d}t^2 + \mathrm{d}\vec{x}^2, \tag{2}$$

are always allowable because $\Sigma = 0$. For Lorentz metrics,

$$\mathrm{d}s^2 = -\mathrm{d}t^2 + \mathrm{d}\vec{x}^2, \tag{3}$$

since $\Sigma = \pi$, they lie on the boundary of the allowable domain of complex metrics (see also the concrete example in (4) below).

Later, Witten proposed to investigate KS's criterion in various interesting examples, including quantum gravity [4], noting that the complex metrics that have proven useful, e.g. complexified black holes, satisfy KS's conditions, while some pathological metrics, e.g. the complex wormholes, do not satisfy KS's conditions. After the proposals in [1, 4], there has been much recent interest in studying the consequences of allowable complex spacetime metrics in various contexts [5–11]. Note that the allowable complex metrics

J. Stat. Mech. (2024) 103103

have also been previously used as a regularization scheme in different contexts, including the analysis of gravitational entropy and the real-time thermal physics [12–14].

In this work, we will explore the consequences of allowable complex metrics in the context of non-equilibrium dynamics in quantum field theories. In particular, we consider the following complex spacetime metrics [4]:

$$\mathrm{d}s_{\pm}^2 = -(1 \mp i\epsilon)^2\,\mathrm{d}t^2 + \mathrm{d}\vec{x}^2, \quad \epsilon > 0. \tag{4}$$

One can find that $\Sigma \in (0, \pi)$ and it satisfies KS's criteria in (1). It is noted that for an allowable metric, $\sqrt{\det g}$ has a positive real part [1, 4]. Therefore, the two choices of signs in (4) differ by the sign of $\sqrt{\det g}$ with $\sqrt{\det g} = \pm i(1 \mp i\epsilon)$, where the real part of $\sqrt{\det g}$ is always positive. As we approach the Lorentzian metric in (3) by taking $\epsilon \to 0$, $\sqrt{\det g}$ approaches the positive or negative imaginary axis, depending on the sign in $\pm i\epsilon$. These two choices correspond to the time propagation by $\exp(-iHt - \epsilon Ht)$ and $\exp(+iHt - \epsilon Ht)$, respectively [4], where H is the Hamiltonian. In this work, these two choices will be used in the time evolution of certain initial states $|\psi_0\rangle$ and $\langle\psi_0|$, respectively. More explicitly, we have

$$|\psi(t)\rangle = e^{-iHt-\epsilon Ht}|\psi_0\rangle, \quad \epsilon > 0, \tag{5}$$

and the complex conjugate $\langle\psi(t)| = \langle\psi_0|e^{+iHt-\epsilon Ht}$. Apparently, this time evolution is non-unitary, where the factor $e^{-\epsilon Ht}$ introduces a damping effect that tends to evolve the wave function to the ground state of H. In this work, we hope to understand what universal features could appear in such non-unitary time evolutions.

Another motivation of this work is to make a connection to the non-unitary time evolution in open quantum systems, where the non-unitary dynamics are caused by the coupling to the measurement apparatus or, more generally, the environment. Some interesting examples include, to name a few, measurement-induced phase transitions [15–18] and long-range entangled state preparation [19–22]. In particular, it has been demonstrated that the measurements of quantum many-body states are related to non-unitary time evolutions; see, e.g. [23–34] for recent works on this topic.

We also note some recent numerical works on complex-time evolution [35–37] in lattice systems and tensor-network states, which are closely related to this work. The goal of these studies was to provide an efficient numerical way to simulate quantum systems, while in our work we are mainly interested in the exactly solvable quantum field theories and universal features in the non-unitary time evolutions.

Before we move on to the concrete setup, we want to emphasize that there are other types of non-unitary time evolutions, such as the time evolution determined by Lindblad master equations. For free-fermion/boson systems, such non-unitary time evolutions may be exactly solvable when certain conditions are satisfied [38–40]; see also recent progress in [41–45]. Although we mainly focus on the time evolution of the form in (5) in this work, in the next parts of this series, for different motivations, we will study other types of exactly solvable non-unitary time evolutions.

J. Stat. Mech. (2024) 103103

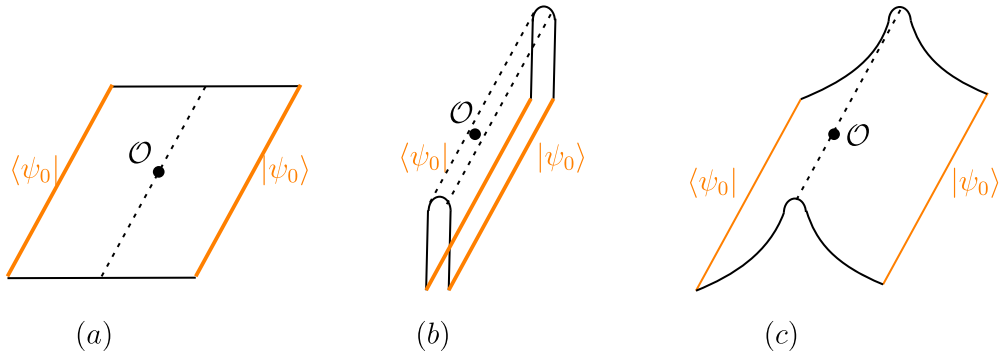

Figure 1. Path integral of one-point function with different spacetime metrics (see the main text for details). (a) Euclidean metric, (b) Lorentz metric, and (c) complex metric.

1.2. Setup

Now let us introduce the non-unitary time evolution of a conformal field theory (CFT) after a global/local quantum quench within the complex spacetime metrics. In general, we consider a given initial state $|\psi_0\rangle$. Then, at $t=0$, we evolve this initial state in (5) with a CFT Hamiltonian[4]:

$$|\psi(t)\rangle = e^{-iH_{\rm CFT}(1-i\epsilon)t}|\psi_0\rangle, \quad \epsilon > 0, \tag{6}$$

where we fix the sign of ϵ in (6) to be positive to ensure that it leads to a convergent path integral. Note that the complex conjugate of this state is $\langle\psi(t)| = \langle\psi_0| e^{iH_{\rm CFT}(1+i\epsilon)t}$. If $\epsilon=0$, it reduces to the real-time evolution, which is unitary. For $\epsilon>0$, the time evolution becomes *non-unitary*.

We will mainly use the path-integral approach to study the complex-time evolution in (6). As an illustration, let us consider the one-point function for the local operator $\mathcal{O}$ in different metrics. First, in the Euclidean metric, to describe $\langle\psi_0|\mathcal{O}(\tau)|\psi_0\rangle = \langle\psi_0|e^{-H\tau}\mathcal{O}e^{-H\tau}|\psi_0\rangle$, we need to consider a path integral that propagates the initial state $|\psi_0\rangle$ in the imaginary time direction to construct a factor $e^{-H\tau}$, after which we insert the operator $\mathcal{O}$ and then propagate the state in the imaginary time direction to construct another factor $e^{-H\tau}$, as shown in figure 1(a). Second, in the Lorentz metric, to describe $\langle\psi_0|\mathcal{O}(t)|\psi_0\rangle = \langle\psi_0|e^{-iHt}\mathcal{O}e^{-iHt}|\psi_0\rangle$, we consider a path integral that propagates the states $|\psi_0\rangle$ forward by a time t to obtain the factor e^{-iHt}. Then we insert the operator $\mathcal{O}$ and propagate the state backward in time to construct the factor e^{iHt}, as shown in figure 1(b). Third, in the complex metric, we consider the one-point function $\langle\psi_0|e^{iHt-\epsilon Ht}\mathcal{O}e^{-iHt-\epsilon Ht}|\psi_0\rangle$. As shown in figure 1(c), the path integral propagates the state $|\Psi\rangle$ both forward and also in the imaginary time direction to obtain the factor $e^{-iHt-\epsilon Ht}$. After inserting the operator $\mathcal{O}$, the path integral propagates the state backward and at the same time in the imaginary time direction to obtain the factor $e^{+iHt-\epsilon Ht}$.

[4] It is emphasized that here ϵ is not necessarily small—it is a real number that can be arbitrarily large.

J. Stat. Mech. (2024) 103103

Next, for the different quantum quenches considered in this work, they correspond to different choices of initial states $|\psi_0\rangle$ in (6). The initial states that we will consider are the same as those in [46, 47], except that we are now interested in the complex-time evolution.

In the global quantum quench, we choose the initial state $|\psi_0\rangle$ as a short-range entangled state, which may be viewed as the ground state of a gapped Hamiltonian. In the context of CFT, such an initial state can be represented by a regularized conformal boundary state $e^{-\frac{\beta}{4}H_{\rm CFT}}|B\rangle\rangle$, where β is a positive real number and $|B\rangle\rangle$ is a conformal boundary state. We study two cases as follows. (1) The total system is of an infinite length defined on $(-\infty,+\infty)$ and the subsystem A is chosen as $A=[0,+\infty)$. (2) The total system is semi-infinite defined on $[0,+\infty)$ and the subsystem A is chosen as a finite interval at the end with $A=[0,l)$.

In the local quantum quench, we choose the initial state $|\psi_0\rangle$ as the tensor product of ground states of two decoupled CFTs defined on $(-\infty,0)$ and $(0,+\infty)$, respectively, i.e. $|\psi_0\rangle=e^{-\lambda H_{\rm CFT}}|G_L\rangle\otimes|G_R\rangle$, where $|G_{L/R}\rangle$ is the ground state of the CFT on the left/right side and the factor $e^{-\lambda H_{\rm CFT}}$ with $\lambda>0$ playing the role of regularization. At $t=0$, we change the Hamiltonian locally by coupling the two CFTs at their ends at $x=0$, such that the new Hamiltonian $H_{\rm CFT}$ defined on $(-\infty,+\infty)$ is translationally invariant in space. The subsystem is chosen as $A=[0,+\infty)$.

Another setup we will consider in this work is the exactly solvable Floquet CFT [48], i.e. a CFT under periodic driving, where one deforms the Hamiltonian density periodically in time. The minimal setup is based on a two-step driving:

$$|\psi(n)\rangle=\left(e^{-iH_0T_0}e^{-iH_1T_1}\right)^n|\psi_0\rangle, \tag{7}$$

where H_0 and H_1 are non-commuting Hamiltonians, and T_0 (T_1) is the corresponding driving time. Here, the driving Hamiltonians H_0 and H_1 are obtained from the uniform CFT Hamiltonian by a spatial deformation as $H_i=\int f_i(x)T_{00}(x)\,{\rm d}x$[5], where $f_i(x)$ is an arbitrary smooth real function, and $T_{00}(x)$ is the Hamiltonian density. If $f(x)$ is of the simple form $f(x)=a+b\cos\frac{2\pi x}{l}+c\sin\frac{2\pi x}{l}$, where l characterizes the wavelength of deformation, one finds that the generators of the driving Hamiltonians form an ${\rm SL}(2,\mathbb{R})$ algebra[6]. Then the operator evolution in a Floquet CFT is described by a Möbius transformation, which is the underlying reason for the exact solvability of this setup. The properties of this exactly solvable Floquet CFT as well as its generalization have been extensively studied recently [48–71]; see also [72–80] for its holographic dual. In this work, we will generalize this Floquet CFT setup to a complex-time evolution, as follows:

$$|\psi(n)\rangle=\left(e^{-i(1-i\epsilon)H_0T_0}e^{-iH_1T_1}\right)^n|\psi_0\rangle. \tag{8}$$

[5] More generally, the deformed Hamiltonian has the form $H_i=\int f_i(x)T(x){\rm d}x+\int g_i(x)\overline{T}(x){\rm d}x$, where $f_i(x)$ and $g_i(x)$ are smooth real functions that are independent from each other, and $T(x)$ and $\overline{T}(x)$ are holomorphic and anti-holomorphic stress–energy tensors [49].

[6] For a general choice of $f(x)$, the underlying algebra is Virasoro algebra.

J. Stat. Mech. (2024) 103103

Here we introduce the complex time only in the time evolution with H_0. The motivation is straightforward: on the one hand, by tuning the system to the heating phase of a Floquet CFT [48], the state will evolve into a highly excited state of H_0. On the other hand, the damping factor $e^{-\epsilon H_0 T_0}$ tends to evolve the system back to the ground state of H_0. This competition between driving and damping may result in a steady state.

Before we leave this section, let us introduce several concepts that will be used to characterize the non-equilibrium dynamics in the above setups. One important concept we will study is the so-called entanglement Hamiltonian or modular Hamiltonian, which is related to the reduced density matrix $\rho_A = \mathrm{Tr}_{\overline{A}}(\rho)$ of a subsystem A as

$$\rho_A = e^{-2\pi K_A} \quad \text{or} \quad K_A = -\frac{1}{2\pi}\log\rho_A. \tag{9}$$

Here, $\overline{A}$ is the complement of A in the whole system. In general, the entanglement Hamiltonian K_A is non-local and it is challenging to write down the explicit form of K_A. However, there are a few cases where the analytical form of K_A can be obtained. An important example is when the theory is defined on the whole of the flat Minkowski space, the entanglement Hamiltonian is the boost generator for the half-plane $x_1 > 0$, i.e. $K_A = \int_{x_1>0} x_1 T_{00}(x)\mathrm{d}^{d-1}x$ [81, 82]. Another solvable case is the chiral free-fermion system, where the entanglement Hamiltonian can be obtained by using the resolvent method [83–85]. In the context of $(1+1)$-dimensional CFTs, it was shown that if the path integral of the reduced density matrix is conformally equivalent to an annulus (or cylinder), then the entanglement Hamiltonians can always be written as an integral over the energy–momentum tensor times a local weight, as follows [86]:

$$K_A(t) = \frac{1}{2\pi}\int_a^b \beta_E(x,t)\, T(x-t)\,\mathrm{d}x + \frac{1}{2\pi}\int_a^b \overline{\beta}_E(x,t)\,\overline{T}(x+t)\,\mathrm{d}x, \tag{10}$$

where $A = [a, b]$ is the subsystem. For the exactly solvable setups as studied in this work, all the entanglement Hamiltonians (for a single interval) are of the form in (10). Here, the local weights $\beta_E(x,t)$ and $\overline{\beta}_E(x,t) \in \mathbb{R}$ in (10) are called the (inverse) entanglement temperatures. A higher entanglement temperature $1/\beta_E(x)$ (or $1/\overline{\beta}_E(x)$) indicates that there is a stronger entanglement between the region near x and the subsystem $\overline{A}$.

The spectrum of K_A, also called the entanglement spectrum, is useful for characterizing and classifying quantum many-body states [87–91]. The entanglement spectrum determines all the Rényi entropies and von Neumann entropy as follows:

$$S_A^{(n)} = \frac{1}{1-n}\log\mathrm{Tr}_A(\rho_A^n) = \frac{1}{1-n}\log\left(\mathrm{Tr}_A e^{-2\pi n K_A}\right), \tag{11}$$

and

$$S_A = -\mathrm{Tr}_A(\rho_A\log\rho_A) = 2\pi\,\mathrm{Tr}_A\left(K_A e^{-2\pi K_A}\right). \tag{12}$$

J. Stat. Mech. (2024) 103103

1.3. Summary of results

Let us first give a brief summary of the main results in this work. For the above setups of quantum quenches in complex spacetime metrics, we can obtain analytical results for the time evolution of the entanglement Hamiltonian, entanglement spectrum, entanglement entropy and energy density at an arbitrary time.

The complex-time evolutions of the entanglement Hamiltonians $K_A(t)$ and entanglement spectrum for the subsystem A are qualitatively different from those in a real-time evolution; see, e.g. equations (28), (48) and (65) for the concrete expressions of $K_A(t)$ after different quantum quenches.

The entanglement entropy evolution in a complex spacetime metric and the comparison with the case of the Lorentzian metric can be summarized as follows:

1. An infinite system over $(-\infty,+\infty)$ after a global quench, with the subsystem $A=[0,+\infty)$:

$$\begin{cases} \text{Lorentzian metric:} & S_A(t)\simeq \frac{\pi c}{3\beta}t, \quad t\to\infty, \\ \text{Complex metric:} & S_A(t)\simeq \frac{c}{6}\log t, \quad t\to\infty. \end{cases} \tag{13}$$

   Here, β is a finite length scale that is introduced in the initial state, which characterizes the correlation length of the initial state, and c is the central charge of the CFT. Hereafter, for $t\to\infty$ or the long time limit, it means t is much larger than any other finite length scales in the problem. For example, here in the Lorentzian metric, $t\to\infty$ corresponds to $t\gg\beta$, while in the complex metric it corresponds to $t\gg\beta/\epsilon$.

2. A semi-infinite system over $(0,+\infty)$ after a global quench, with the subsystem $A=[0,l]$:

$$\begin{cases} \text{Lorentzian metric:} & S_A(t)\simeq \frac{\pi c}{3\beta}l, \quad t\to\infty, \\ \text{Complex metric:} & S_A(t)\simeq \frac{c}{6}\log l, \quad t\to\infty. \end{cases} \tag{14}$$

3. Local quench. The total system is $(-\infty,+\infty)$, and the subsystem is $A=[0,+\infty)$:

$$\begin{cases} \text{Lorentzian metric:} & S_A(t)\simeq \frac{c}{3}\log t, \quad t\to\infty, \\ \text{Complex metric:} & S_A(t)\simeq \frac{c}{6}\log t, \quad t\to\infty. \end{cases} \tag{15}$$

In both the global and local quenches, the local energy density $\langle T_{00}(x,t)\rangle$ will decay to zero in time as $1/t^2$; see, e.g. the plots in figures 5, 8 and 11, as well as the concrete expressions of $\langle T_{00}(x,t)\rangle$ in equations (45), (57), (58) and (76), respectively. One particularly interesting result is for the case of local quench in section 4, where two pulses of energy density are generated after the quench. One can see clearly how these two pulses of energy density die out as they propagate in space due to the complex spacetime metric, as shown in figure 11.

For each case introduced above, we also performed a numerical calculation on the entanglement entropy and energy density evolution based on free-fermion lattice models, and find a good agreement with the field theory results.

J. Stat. Mech. (2024) 103103

Moreover, we study the effect of complex spacetime metrics in a time-dependent driven quantum critical system, more specifically in a Floquet CFT [48]. Since the complex-time evolution introduces a damping effect, there will be a competition between the driving and damping in a driven system. Based on a numerical study of the Floquet CFT in complex metrics, we find that this competition results in a steady state, where the interesting patterns of entanglement and energy density in space are inherited from those of a Floquet CFT in the real-time evolution.

The structure of the rest of the paper is organized as follows: we consider exactly solvable time evolutions in a CFT after different setups of quantum quenches. In section 2, we study an infinite system after a global quench, where the subsystem is chosen as a semi-infinite system. In section 3, we study a semi-infinite system after a global quench, and the subsystem of a finite length is at the end of this semi-infinite system. In section 4, we study a local quantum quench by joining two CFTs at their ends suddenly. In section 5, we consider a periodically driven quantum critical system on a lattice in a complex spacetime metric, with the goal of studying the competition between driving and damping. In appendix, we give some details on the complex-time evolution in a free-fermion lattice model.

2. Global quench with complex metrics: an infinite system

For a CFT after a global quantum quench, here we consider the setup introduced in [46]. We start from an initial state of the following form:

$$|\psi_0\rangle = e^{-\frac{\beta}{4}H_{\rm CFT}}|B\rangle\rangle, \tag{16}$$

where $|B\rangle\rangle$ is a conformal boundary state, noting that there is no scale in the conformal boundary state, $|B\rangle\rangle$ is not normalizable itself and has zero real-space entanglement [92]. By introducing the regularization factor $e^{-\frac{\beta}{4}H_{\rm CFT}}$ in (16), $|\psi_0\rangle$ is normalizable and has a finite real-space entanglement. Physically, β characterizes the correlation length of the initial state.

In the Lorentz metric, the state after a quantum quench is $|\psi(t)\rangle = e^{-iH_{\rm CFT}t}|\psi_0\rangle$. The time-dependent density matrix can be written as

$$\rho(t) = e^{-iH_{\rm CFT}t}e^{-\frac{\beta}{4}H_{\rm CFT}}|B\rangle\rangle\langle\langle B|e^{-\frac{\beta}{4}H_{\rm CFT}}e^{iH_{\rm CFT}t}. \tag{17}$$

Then the path integral of $\rho_A = {\rm Tr}_{\overline{A}}\rho(t)$ for a subsystem $A = [x_1, x_2]$ can be represented in figure 2(b) by sewing together the degrees of freedom in region $\overline{A}$. Here, the width of the strip in figure 2(b) is $\beta/2$, which is introduced by the regularization factor in (16), and the branch cut (blue lines) corresponds to the subsystem A[7]. To study ρ_A, it is convenient to take the analytical continuation $\tau = it$ first, by writing $\rho(t)$ as

$$\rho(\tau) = e^{-\left(\frac{\beta}{4}+\tau\right)H_{\rm CFT}}|B\rangle\rangle\langle\langle B|e^{-\left(\frac{\beta}{4}-\tau\right)H_{\rm CFT}}. \tag{18}$$

[7] For readers who are not familiar with the path integral interpretation of reduced density matrix, see the recent reviews [93, 94].

J. Stat. Mech. (2024) 103103

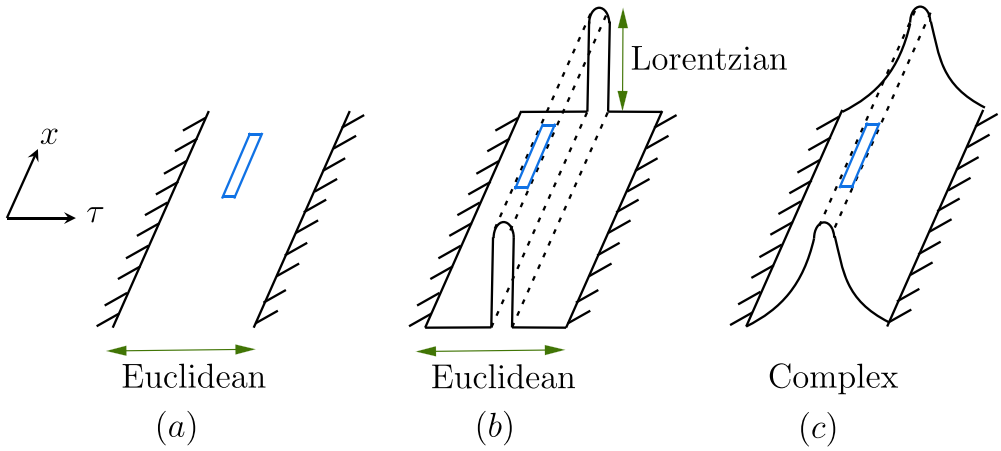

Figure 2. Path integral of the reduced density matrix ρ_A after a global quench in a CFT with (a) Euclidean, (b) partial Euclidean and partial Lorentz, and (c) complex spacetime metrics. The fields living on the upper and lower edges of the branch cut (in blue) correspond to the rows and columns of ρ_A.

The path integral of $\rho_A(\tau)$ corresponds to the configuration in the Euclidean space in figure 2(a). Then, one can evaluate $\rho_A(t)$ or equivalently the entanglement Hamiltonian $K_A(t)$ by taking $\tau \to it$ in the final step [46, 86].

We are now interested in the complex-time evolution in (6), and the density matrix $\rho(t)$ can be written as

$$\rho(t) = e^{-iH_{\rm CFT}t} e^{-\left(\frac{\beta}{4}+\epsilon t\right)H_{\rm CFT}} |B\rangle\rangle\langle\langle B| e^{-\left(\frac{\beta}{4}+\epsilon t\right)H_{\rm CFT}} e^{iH_{\rm CFT}t}. \tag{19}$$

The path integral of $\rho_A(t) = {\rm Tr}_{\overline{A}}\rho(t)$ corresponds to the configuration in figure 2(c). To evaluate $\rho_A(t)$ as well as other physical quantities, we define the two-time density matrix $\rho(t_1, t_2)$ as

$$\rho(t_1,t_2) = e^{-iH_{\rm CFT}t_2} e^{-\left(\frac{\beta}{4}+\epsilon t_1\right)H_{\rm CFT}} |B\rangle\rangle\langle\langle B| e^{-\left(\frac{\beta}{4}+\epsilon t_1\right)H_{\rm CFT}} e^{iH_{\rm CFT}t_2}. \tag{20}$$

Then, by taking $\tau_2 = it_2$ and $\tau_1 = t_1$, we have

$$\rho(\tau_1,\tau_2) = e^{-\left(\frac{\beta}{4}+\epsilon\tau_1+\tau_2\right)H_{\rm CFT}} |B\rangle\rangle\langle\langle B| e^{-\left(\frac{\beta}{4}+\epsilon\tau_1-\tau_2\right)H_{\rm CFT}}, \tag{21}$$

The path integral of $\rho(\tau_1, \tau_2)$ as well as the reduced density matrix $\rho_A(\tau_1, \tau_2) = {\rm Tr}_{\overline{A}}\rho(\tau_1, \tau_2)$ is defined in the Euclidean space in figure 2(a). In the final step, by considering the following analytical continuation,

$$\tau_1 \to t \quad \text{and} \quad \tau_2 \to it, \tag{22}$$

one can obtain the time evolution of $\rho_A(t) = {\rm Tr}_{\overline{A}}\rho(t)$ and the corresponding entanglement Hamiltonian $K_A(t)$, where $\rho(t)$ is defined in (19).

J. Stat. Mech. (2024) 103103

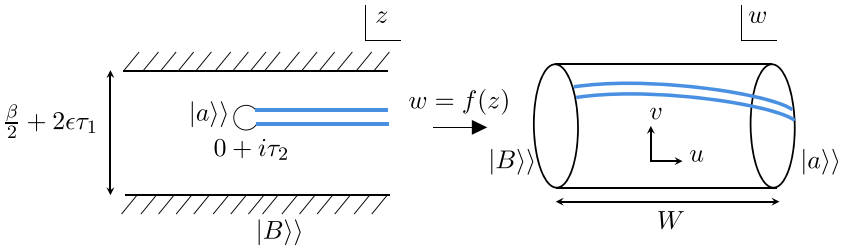

Figure 3. The path integral of $\rho_A = \mathrm{Tr}_{\overline{A}}\rho(\tau_1,\tau_2)$ for $A=[0,+\infty)$ in the Euclidean space. The width of the strip is $\beta/2+2\epsilon\tau_1$, with the two boundaries located along $\mathrm{Im}\, z=-\beta/4-\epsilon\tau_1$ and $\beta/4+\epsilon\tau_1$, respectively. The branch cut corresponding to subsystem A is along $C=\{i\tau_2+x, x\geqslant 0\}$. A small disk of radius ϵ_0 is removed at the entanglement point $z_0=0+i\tau_2$, with a conformal boundary condition $|a\rangle\rangle$ imposed along the boundary of this removed disk. After a conformal mapping $w=f(z)$, the strip (left) is mapped to a cylinder (right) of length W in the $\mathrm{Re}\, w$ direction. The circumference of the cylinder along the $\mathrm{Im}\, w$ direction is 2π.

2.1. Entanglement Hamiltonian and entanglement spectrum evolution

Let us start from $\rho_A(\tau_1,\tau_2)$ in the Euclidean space, as shown in figure 3. Here, $\rho_A(\tau_1,\tau_2)$ is obtained from $\rho(\tau_1,\tau_2)$ in (21) by sewing together the degrees of freedom in $\overline{A}$, and the branch cut along $C=\{i\tau_2+x, x\geqslant 0\}$ corresponds to the subsystem $A=[0,+\infty)$.

Following the method in [86], we consider the conformal mapping

$$w=f(z)=\log\left(\frac{\sinh\left[\pi\left(z-i\tau_2\right)/\left(\beta+4\epsilon\tau_1\right)\right]}{\cosh\left[\pi\left(z+i\tau_2\right)/\left(\beta+4\epsilon\tau_1\right)\right]}\right), \tag{23}$$

which maps $\rho_A(\tau_1,\tau_2)$ in the z-plane to a w-cylinder, where $w=u+iv$, as shown in figure 3. The entanglement Hamiltonian K_A after the above conformal mapping $w=f(z)$ can be considered as the generator of translation along the cylinder in the v-direction, i.e.

$$K_A=-2\pi\int T_{vv}\,\mathrm{d}u, \tag{24}$$

where the integral is along a constant v, and T_{vv} is the Hamiltonian density in Euclidean signature. One can further write K_A in terms of the holomorphic (anti-holomorphic) component of the stress–energy tensor T ($\overline{T}$) as

$$K_A=\int_{f(C)}T(w)\,\mathrm{d}w+\int_{\overline{f(C)}}\overline{T}(\overline{w})\,\mathrm{d}\overline{w}, \tag{25}$$

where we have considered the convention $T_{vv}=-(T+\overline{T})/2\pi$. By mapping back to the original z-plane, the entanglement Hamiltonian becomes

$$K_A=\int_C\frac{T(z)}{f'(z)}\mathrm{d}z+\int_{\overline{C}}\frac{\overline{T}(\overline{z})}{\overline{f'(z)}}\mathrm{d}\overline{z}. \tag{26}$$

J. Stat. Mech. (2024) 103103

Here, we have ignored the Schwarzian derivative term, since it will be canceled in the calculation of entanglement entropy by introducing the normalization of ρ_A. As a remark, the above procedure for studying the entanglement Hamiltonian is not limited to the setup of a global quantum quench in figure 3. The same procedure can be applied to other setups in sections 3 and 4 later.

Based on (23) and (26), we can obtain the concrete form of the entanglement Hamiltonian as follows:

$$\begin{aligned} K_A = &\frac{\beta+4\epsilon\tau_1}{\pi}\int_0^\infty \frac{\sinh\left[\pi x/\left(\beta+4\epsilon\tau_1\right)\right]\cdot\cosh\left[\pi\left(x+2i\tau_2\right)/\left(\beta+4\epsilon\tau_1\right)\right]}{\cosh\left[2\pi i\tau_2/\left(\beta+4\epsilon\tau_1\right)\right]}T\left(x+i\tau_2\right)\mathrm{d}x \\ &+\frac{\beta+4\epsilon\tau_1}{\pi}\int_0^\infty \frac{\sinh\left[\pi x/\left(\beta+4\epsilon\tau_1\right)\right]\cdot\cosh\left[\pi\left(x-2i\tau_2\right)/\left(\beta+4\epsilon\tau_1\right)\right]}{\cosh\left[2\pi i\tau_2/\left(\beta+4\epsilon\tau_1\right)\right]}\overline{T}\left(x-i\tau_2\right)\mathrm{d}x. \end{aligned} \tag{27}$$

By taking the analytical continuation $\tau_1 \to t$ and $\tau_2 \to it$, the entanglement Hamiltonian becomes

$$\begin{aligned} K_A\left(t\right) = &\frac{\beta+4\epsilon t}{\pi}\int_0^\infty \frac{\sinh\left[\pi x/\left(\beta+4\epsilon t\right)\right]\cdot\cosh\left[\pi\left(x-2t\right)/\left(\beta+4\epsilon t\right)\right]}{\cosh\left[2\pi t/\left(\beta+4\epsilon t\right)\right]}T\left(x-t\right)\mathrm{d}x \\ &+\frac{\beta+4\epsilon t}{\pi}\int_0^\infty \frac{\sinh\left[\pi x/\left(\beta+4\epsilon t\right)\right]\cdot\cosh\left[\pi\left(x+2t\right)/\left(\beta+4\epsilon t\right)\right]}{\cosh\left[2\pi t/\left(\beta+4\epsilon t\right)\right]}\overline{T}\left(x+t\right)\mathrm{d}x. \end{aligned} \tag{28}$$

This entanglement Hamiltonian fully characterizes the property of subsystem A under a complex-time evolution. There are several remarks in order:

First, by setting $\epsilon = 0$, the entanglement Hamiltonian $K_A(t)$ reduces to the case in a real-time evolution [86].

Second, for the complex-time evolution with $\epsilon > 0$, let us consider the (inverse) entanglement temperature defined in (10). For a general $x \gg \beta$, in the long time limit with $t \gg x$ and $t \gg \beta/\epsilon$, one can find

$$\beta_E\left(x,t\right) \simeq \overline{\beta}_E\left(x,t\right) \simeq 2\pi x, \quad \epsilon > 0, \tag{29}$$

which corresponds to the result in the ground state. This is due to the damping effect introduced by the complex-time evolution. As a comparison, in the real-time evolution with $x \gg \beta$ and $t \gg x$, we have

$$\beta_E\left(x,t\right) \simeq \beta, \quad \overline{\beta}_E\left(x,t\right) \to \infty, \quad \epsilon = 0, \tag{30}$$

where the asymmetry can be understood based on the quasi-particle picture, i.e. the entanglement entropy in A is mainly contributed by the right-moving quasi-particles emitted from the initial state [86].

To have a more straightforward understanding of the time-dependent entanglement Hamiltonian, it is helpful to study its spectrum, i.e. the entanglement spectrum, as follows.

J. Stat. Mech. (2024) 103103

– *Time evolution of entanglement spectrum:*

The spacing of the entanglement spectrum as a function of time t depends on the length $W(t)$ of the cylinder in figure 3 after an analytical continuation $\tau_1 \to t$ and $\tau_2 \to it$:

$$E_i(t) - E_j(t) = \frac{\pi(\Delta_i - \Delta_j)}{W(t)}, \tag{31}$$

where Δ_i are the scaling dimensions of the boundary operators. The length $W(t)$ can be obtained as follows. First, by defining

$$\mathcal{W} = f(i\tau_2 + \infty) - f(i\tau_2 + \epsilon_0), \tag{32}$$

the length of the cylinder in figure 3 has the form

$$W = \mathrm{Re}\,\mathcal{W} = \frac{1}{2}\left(\mathcal{W} + \overline{\mathcal{W}}\right). \tag{33}$$

From (32), it is straightforward to obtain that

$$\mathcal{W} = \log\left(\frac{\cosh\left[\pi\left(\epsilon_0 + 2i\tau_2\right)/\left(\beta + 4\epsilon\tau_1\right)\right]}{\sinh\left[\pi\epsilon_0/\left(\beta + 4\epsilon\tau_1\right)\right]}\right) - i\frac{2\pi\tau_2}{\beta + 4\epsilon\tau_1}. \tag{34}$$

Then based on (33), after an analytical continuation $\tau_1 \to t$ and $\tau_2 \to it$, one can obtain

$$W(t) = \frac{1}{2}\log\left(\frac{\cosh\left[2\pi\epsilon_0/\left(\beta + 4\epsilon t\right)\right] + \cosh\left[4\pi t/\left(\beta + 4\epsilon t\right)\right]}{2\sinh^2\left[\pi\epsilon_0/\left(\beta + 4\epsilon t\right)\right]}\right), \quad \epsilon \geqslant 0. \tag{35}$$

Now let us consider the long time evolution limit $t \to \infty$, or more precisely $t \gg \beta/\epsilon$. The scaling behavior of $W(t)$ depends on whether the time evolution is real ($\epsilon = 0$) or complex ($\epsilon > 0$), as follows:

$$\begin{cases} W(t \to \infty) \sim \frac{2\pi t}{\beta}, & \text{real time evolution}(\epsilon = 0), \\ W(t \to \infty) \sim \log t, & \text{complex time evolution } (\epsilon > 0). \end{cases} \tag{36}$$

Then, based on the relation in (31), one can find that in the long time limit $t \to \infty$,

$$\begin{cases} \text{Spacing of entanglement spectrum} \sim \frac{1}{t}, & \text{real time evolution}\,(\epsilon = 0), \\ \text{Spacing of entanglement spectrum} \sim \frac{1}{\log t}, & \text{complex time evolution}\,(\epsilon > 0). \end{cases} \tag{37}$$

This feature is closely related to the entanglement entropy evolution as discussed in the next subsection.

2.2. Entanglement entropy evolution

As seen from (11) and (12), the Rényi entropy and von Neumann entropy are determined by the entanglement Hamiltonian K_A and its spectrum. In the complex-time evolution of entanglement entropy, the method as used in [86] still works, which we do not repeat

J. Stat. Mech. (2024) 103103

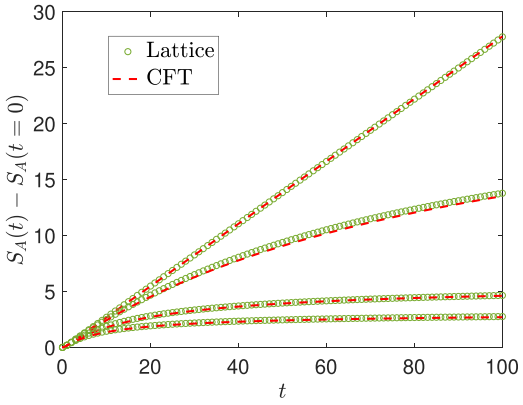

Figure 4. Comparison of complex-time evolution of entanglement entropy $S_A(t)$ after a global quench in lattice system and CFT calculations. The lattice system is defined on $[0, L] = [0, 800]$, and the subsystem is $A = [0, 400]$. The mass term in the lattice model is set as $m = 1/2$ in (91). From top to bottom, we choose ϵ (which characterizes the imaginary part of the complex time) as $\epsilon = 0$ (Lorentz metric), 0.01, 0.05 and 0.1. The CFT result is plotted according to (38) and (35), and the fitting parameters are $\beta = 3.75$ and $\epsilon_0 = 0.1$.

here. One can find that the nth Rényi entropy and von Neumann entropy are related to $W(t)$ in (35) as

$$S_A^{(n)}(t) \simeq \frac{c}{12}\left(1+\frac{1}{n}\right) W(t) - g_a - g_b, \quad S_A(t) \simeq \frac{c}{6} W(t) - g_a - g_b, \tag{38}$$

where g_a and g_b are boundary entropies [95]. Here, we are mainly interested in the leading term which is proportional to $W(t)$, the expression of which was already given in (35). Note that the relation in (38) can be applied to other cases if the reduced density matrix ρ_A can be conformally mapped to a cylinder [86].

As shown in figure 4, we compare the CFT results in (38) and (35) and a numerical calculation based on the free-fermion lattice system (see appendix for more details), and one finds that the agreement is remarkable. In the real-time evolution ($\epsilon = 0$), one can find that the entanglement entropy grows linearly in time [46]. In the complex-time evolution($\epsilon > 0$), the entanglement entropy evolution is suppressed in time. As we increase ϵ, since the damping effect is stronger, one finds that $S_A(t)$ is more suppressed, as expected.

In the long time limit, based on the behavior of $W(t)$ in (36), one can find

$$\begin{cases} S_A(t\to\infty) \simeq \frac{c}{3}\cdot\frac{\pi t}{\beta}, & \text{real time evolution}\,(\epsilon = 0), \\ S_A(t\to\infty) \simeq \frac{c}{6}\log t, & \text{complex time evolution}\,(\epsilon > 0). \end{cases} \tag{39}$$

The complex-time evolution of entanglement entropy is qualitatively different from that in a real-time evolution.

J. Stat. Mech. (2024) 103103

2.3. Energy density evolution

Now let us consider the local energy density evolution, i.e. $\langle T_{00}(x,t)\rangle$. In the real-time evolution, it is known that the quench dynamics considered here conserve the energy, with $\langle T_{00}(x,t)\rangle = \frac{\pi c}{6\beta^2}$ [96]. Now, because of the damping effect in the complex-time evolution, it is expected that the energy density will decay in time.

More concretely, let us consider the one-point function $\langle T(z)\rangle$, which corresponds to inserting a holomorphic stress-tensor energy operator T at $z = x + i\tau_2$ in the strip configuration in figure 3 (with the branch cut now removed). By considering the conformal mapping

$$w = f(z) = e^{\frac{2\pi}{\beta+4\epsilon\tau_1}\cdot z}, \tag{40}$$

which maps the z-strip to the w upper half-plane, as follows:

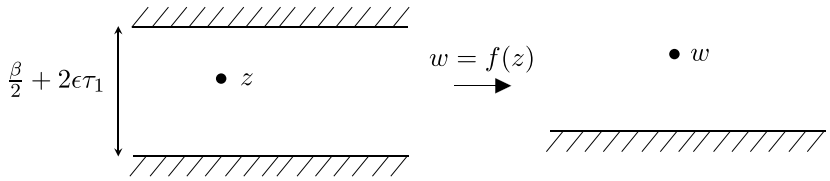

(41)

the stress–energy tensor transforms as

$$T_{\text{strip}}(z) = \left(\frac{\mathrm{d}z}{\mathrm{d}w}\right)^{-2} T_{\text{UHP}}(w) - \frac{c}{12}\{w,z\}, \tag{42}$$

where $\{w,z\}$ is the Schwarzian derivative defined by

$$\{w,z\} := \frac{\mathrm{d}^3 w/\mathrm{d}z^3}{\mathrm{d}w/\mathrm{d}z} - \frac{3}{2}\left(\frac{\mathrm{d}^2 w/\mathrm{d}z^2}{\mathrm{d}w/\mathrm{d}z}\right)^2. \tag{43}$$

Since $\langle T_{\text{UHP}}(w)\rangle = 0$, we have $\langle T_{\text{strip}}(z)\rangle = -\frac{c}{12}\{w,z\}$, based on which and (40) one can obtain (after an analytical continuation $\tau_1 \to t$ and $\tau_2 \to it$)

$$\langle T_{\text{strip}}(x,t)\rangle = \frac{c}{24}\cdot\frac{\pi^2}{\left(\frac{\beta}{2}+2\epsilon t\right)^2}. \tag{44}$$

One can obtain the same expression for $\langle \overline{T}_{\text{strip}}(x,t)\rangle$. Therefore, the local energy density evolves in time as

$$\langle T_{00}(x,t)\rangle = \frac{1}{2\pi}\left[\langle T(x,t)\rangle + \langle \overline{T}(x,t)\rangle\right] = \frac{\pi c}{24\left(\frac{\beta}{2}+2\epsilon t\right)^2}. \tag{45}$$

For $\epsilon = 0$, we reproduce the real-time evolution result in [96, 97]. For $\epsilon > 0$, the energy density decays in time due to the complex time. As $t \to +\infty$, the energy density decays

J. Stat. Mech. (2024) 103103

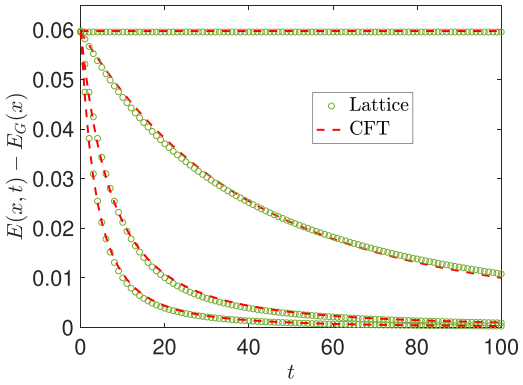

Figure 5. Comparison of energy density evolution $E(x,t)-E_G(x)$ after a global quench in complex spacetime metric in a free-fermion lattice system (green circles) and in a CFT calculation (red dashed lines). Here, $E_G(x)$ is the energy density in the ground state of a CFT. The lattice system is defined on $[0,L]=[0,800]$. The mass term used in the initial state of the lattice model is set as $m=1/2$ in (91). The energy density is calculated by considering the average $\frac{1}{l}\int_{L/2-l/2}^{L/2+l/2}E(x,t)\mathrm{d}x$ with $l=100$ in the lattice calculation. From top to bottom, we have $\epsilon=0$, 0.01, 0.05 and 0.1. The fitting parameter in CFT is $\beta=2.96$.

to the ground state value in time as $1/t^2$, which is consistent with our analysis of the entanglement Hamiltonian evolution in section 2.1.

A comparison of the energy density evolution in lattice and CFT calculations for different values of ϵ can be found in figure 5, where one can find a remarkable agreement. See appendix for more details on the lattice calculations.

3. Global quench with complex metrics: a semi-infinite system

Now we consider a semi-infinite system in $[0,+\infty)$ after a global quantum quench, where the subsystem $A=[0,l]$ is at the end of this semi-infinite system. In the real-time evolution, it is known that the entanglement entropy evolution as well as other quantities depend on the length scale l [96]. For example, the entanglement entropy $S_A(t)$ grows linearly in time if $t<l$, and saturates if $t>l$. Also, as studied in [98, 99], for $t>l$, the entanglement Hamiltonian and entanglement spectrum for subsystem $A=[0,l]$ approach those in a thermal ensemble at a finite temperature exponentially fast in time. Here, we will generalize this setup to the case of a complex-time evolution.

3.1. Entanglement Hamiltonian and entanglement spectrum evolution

Let us first consider the path integral of $\rho_A(\tau_1,\tau_2)=\mathrm{Tr}\rho(\tau_1,\tau_2)$ in Euclidean spacetime. Here, $\rho(\tau_1,\tau_2)$ has the same definition as in (21) except that now the initial state is

J. Stat. Mech. (2024) 103103

defined over a semi-infinite system. Pictorially, the path integral of $\rho_A(\tau_1,\tau_2)$ corresponds to a half strip in the z-plane as follows:

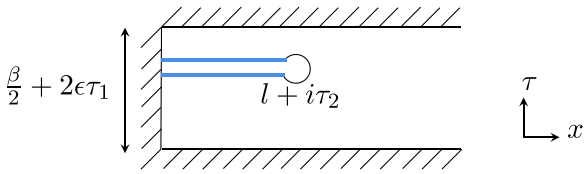

(46)

There are three boundaries here: the first two boundaries that correspond to the initial state are along $\mathrm{Im}\, z=-\beta/4-\epsilon\tau_1$ and $\mathrm{Im}\, z=\beta/4+\epsilon\tau_1$, respectively. The third boundary along $\mathrm{Re}\, z=0$ corresponds to the physical boundary of the semi-infinite system. The branch cut corresponding to subsystem A is along $C=\{i\tau_2+x, 0\leqslant x\leqslant l\}$. To introduce a UV cutoff, a small disk of radius ϵ_0 is removed at the entangling point at $z=l+i\tau_2$.

Next, we map $\rho_A(\tau_1,\tau_2)$ in (46) to a w-cylinder (see the right plot in figure 3) by using the following two-step conformal mapping:

$$\begin{cases} \xi(z) &= \sinh\left(\frac{2\pi z}{\beta+4\epsilon\tau_1}\right), \\ w(\xi) &= -\log\left(\frac{1+\bar{\xi}_0}{1+\xi_0}\cdot\frac{\xi-\xi_0}{\xi+\bar{\xi}_0}\right), \end{cases} \tag{47}$$

where $\xi=\xi(z)$ and $\xi_0=\xi(z_0)$ with $z_0=l+i\tau_2$. Then the entanglement Hamiltonian K_A corresponds to the generator of translation in the direction of $v=\mathrm{Im}\, w$ in the w-cylinder. Based on (26), one can obtain the entanglement Hamiltonian for $A=[0,l]$ at an arbitrary time t as follows (after an analytical continuation $\tau_1\to t$ and $\tau_2\to it$):

$$\begin{aligned} K_A(t) = &\frac{\beta+4\epsilon t}{\pi}\int_l^0 \frac{\sinh\left[\frac{\pi(x-l)}{\beta+4\epsilon t}\right]\cosh\left[\frac{\pi(x-2t+l)}{\beta+4\epsilon t}\right]\sinh\left[\frac{\pi(x+l)}{\beta+4\epsilon t}\right]\cosh\left[\frac{\pi(x-2t-l)}{\beta+4\epsilon t}\right]}{\cosh\left(\frac{2\pi}{\beta+4\epsilon t}t\right)\sinh\left(\frac{2\pi}{\beta+4\epsilon t}l\right)\cosh\left[\frac{2\pi}{\beta+4\epsilon t}(x-t)\right]}T(x,t)\,\mathrm{d}x \\ &+\frac{\beta+4\epsilon t}{\pi}\int_l^0 \frac{\sinh\left[\frac{\pi(x-l)}{\beta+4\epsilon t}\right]\cosh\left[\frac{\pi(x+2t+l)}{\beta+4\epsilon t}\right]\sinh\left[\frac{\pi(x+l)}{\beta+4\epsilon t}\right]\cosh\left[\frac{\pi(x+2t-l)}{\beta+4\epsilon t}\right]}{\cosh\left(\frac{2\pi t}{\beta+4\epsilon t}\right)\sinh\left(\frac{2\pi l}{\beta+4\epsilon t}\right)\cosh\left[\frac{2\pi(x+t)}{\beta+4\epsilon t}\right]}\overline{T}(x,t)\,\mathrm{d}x. \end{aligned} \tag{48}$$

For $\epsilon=0$, one can find that $K_A(t)$ reduces to the result in a real-time evolution in [98]. One main difference between the real-time and complex-time evolutions can be observed in the long time limit. In the real-time evolution with $t\gg\beta$ and $t>l$, the entanglement temperature as defined in (10) is

$$\beta_E(x,t)\simeq\overline{\beta}_E(x,t)\simeq\beta,\quad \epsilon=0. \tag{49}$$

That is, $\rho_A(t)$ for $A=[0,l]$ is the same as that in a thermal ensemble at a finite temperature β^{-1} [98]. In the complex-time evolution with $t\gg l/\epsilon$, however, the entanglement temperature will reach the following steady value:

$$\beta_E(x,t)\simeq\overline{\beta}_E(x,t)\simeq 2\pi\cdot\frac{l^2-x^2}{2l},\quad \epsilon>0. \tag{50}$$

J. Stat. Mech. (2024) 103103

This is nothing but the result for a subsystem $A=[0,l]$ in the ground state of a semi-infinite system in $[0,+\infty)$. It is due to the damping effect introduced by the complex time. For a more intuitive understanding of the time-dependent entanglement Hamiltonian, let us take a closer look at its spectrum.

– *Time evolution of entanglement spectrum:*

By using the same procedure as in section 2.1, one finds that the spacing of the entanglement spectrum is described by (31), where $W(t)$ has the expression

$$W(t)=\log\left\{\frac{2\sinh\left[\frac{2\pi}{\beta+4\epsilon t}\left(l-\frac{\epsilon_0}{2}\right)\right]\cdot\cosh\left(\frac{2\pi t}{\beta+4\epsilon t}\right)}{\sinh\left(\frac{2\pi}{\beta+4\epsilon t}\cdot\frac{\epsilon_0}{2}\right)\cdot\sqrt{2\cosh\left(\frac{2\pi}{\beta+4\epsilon t}\cdot 2l\right)+2\cosh\left(\frac{2\pi}{\beta+4\epsilon t}\cdot 2t\right)}}\right\},\quad \epsilon\geqslant 0. \tag{51}$$

In the real-time evolution ($\epsilon=0$) with $t\gg\beta$, one can find $W(t)$ as [98]

$$W(t)\simeq\begin{cases}\frac{2\pi}{\beta}t, & t<l,\\ \frac{2\pi}{\beta}l, & t>l.\end{cases} \tag{52}$$

That is, the spacing of the entanglement spectrum first decays as $1/t$ for $t<l$, and then saturates at a value that is proportional to l/β.

In the complex-time evolution ($\epsilon>0$), the behavior of $W(t)$ is complicated for a general time t, but it has very simple features in certain limits:

$$W(t)\simeq\begin{cases}\log t, & \beta/\epsilon\ll t<l,\\ \log\left(\frac{2l}{\epsilon_0}\right), & \epsilon t\gg l.\end{cases} \tag{53}$$

That is, if $\beta/\epsilon\ll t<l$, the spacing of the entanglement spectrum will decay as $1/\log t$ in time. For $\epsilon t\gg l$, the spacing of the entanglement spectrum will approach the ground-state value.

As a remark, for certain choices of β and ϵ, the condition $\beta/\epsilon\ll l$ in (53) may not be satisfied. In this case, $W(t)$ does not have a simple scaling behavior for $t<l$.

3.2. Entanglement entropy evolution

Since the reduced density matrix in (46) is conformally equivalent to a cylinder, the Rényi and von Neumann entropies are related to $W(t)$ through the same equation as in (38). Together with (52), one can find that in a real-time evolution, $S_A(t)\simeq\frac{\pi c}{3\beta}t$ for $t<l$, and $S_A(t)\simeq\frac{\pi c}{3\beta}l$ for $t>l$, which can be understood based on the quasi-particle picture [46].

The feature of $S_A(t)$ becomes qualitatively different in the complex-time evolution, as seen in figure 6. More concretely, one can find that:

J. Stat. Mech. (2024) 103103

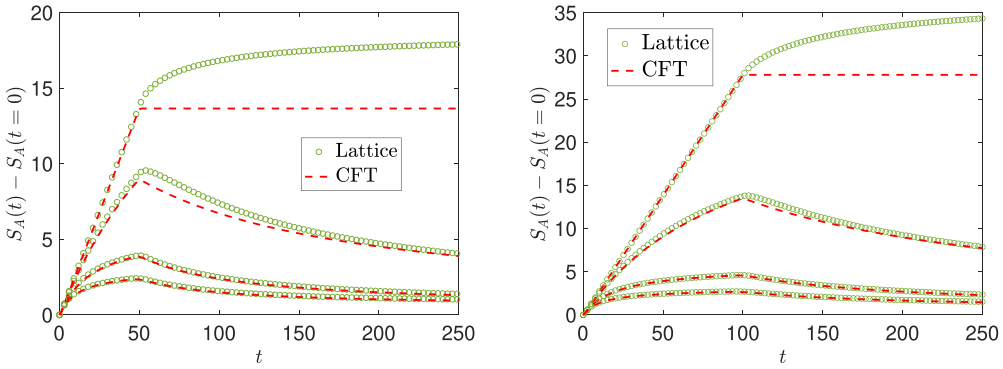

Figure 6. Comparison of complex-time evolution of entanglement entropy $S_A(t)$ after a global quench in lattice system and CFT calculations. Now the subsystem $[0,l]$ is at the end of the total system. The parameters are the same as those in figure 4 but with $A=[0,50]$ (left plot) and $A=[0,100]$ (right plot). In each plot, from top to bottom, we have $\epsilon=0$, 0.01, 0.05 and 0.1.

1. For $t<l$, the entanglement entropy evolution is slower than a linear growth. In particular, if $\beta/\epsilon \ll t<l$, one has

$$S_A(t) \simeq \frac{c}{6}\cdot \log t. \tag{54}$$

   Similar to the discussion near (53), it is possible that $\beta/\epsilon \ll l$ is not satisfied for certain choices of β and ϵ. In this case, $S_A(t)$ does not have a simple form of time dependence as in (54); see, e.g. the exact plot of $S_A(t)$ in figure 6.
2. For $t \gg l/\epsilon$, the entanglement entropy reaches a steady value

$$S_A(t) \simeq \frac{c}{6}\cdot \log\left(\frac{2l}{\epsilon_0}\right), \tag{55}$$

   which is the result for the entanglement entropy of $A=[0,l]$ in the ground state of a semi-infinite CFT on $[0,\infty)$. This is because the excitations injected at $t=0$ will die out due to the damping effect caused by the complex time. Then, in the long time limit $t \gg l/\epsilon$, the state will decay to the ground state of $H_{\rm CFT}$.

3.3. Energy density evolution

The analysis of the energy density evolution is similar to that in section 2.3. Now, in the presence of a physical boundary at $x=0$, there will be a modification of the energy density due to the Casimir effect.

We consider the one-point function $\langle T(z)\rangle$ by inserting a holomorphic stress–energy tensor operator T at $z=x+i\tau_2$ in the half-strip in (46) (with the branch cut removed). Then, with the conformal mapping

$$w=f(z)=\sinh\left(\frac{2\pi z}{\beta+4\epsilon\tau_1}\right), \tag{56}$$

J. Stat. Mech. (2024) 103103

one can map the half-strip in (46) to a right-half-plane (RHP) in the w-coordinate. Since $\langle T_{\rm RHP}(w)\rangle = \langle \overline{T}_{\rm RHP}(\overline{w})\rangle = 0$, one can find $\langle T_{\rm strip}(z)\rangle = -\frac{c}{12}\{w,z\}$, and similarly for $\overline{T}_{\rm strip}(\overline{z})$, where $\{w,z\}$ is the Schwarzian derivative defined in (43). One can obtain

$$\langle T_{\rm strip}\,(x,t)\rangle = -\frac{c}{12}\,\{w,z\} = \frac{\pi^2 c}{6}\cdot\left(\frac{1}{\beta+4\epsilon t}\right)^2\cdot\left[3\tanh^2\frac{2\pi\,(x-t)}{\beta+4\epsilon t}-2\right]. \tag{57}$$

Similarly, we have

$$\langle \overline{T}_{\rm strip}\,(x,t)\rangle = -\frac{c}{12}\,\{w,z\} = \frac{\pi^2 c}{6}\cdot\left(\frac{1}{\beta+4\epsilon t}\right)^2\cdot\left[3\tanh^2\frac{2\pi\,(x+t)}{\beta+4\epsilon t}-2\right]. \tag{58}$$

One can find that the energy density is not uniform in space. Before we move on to the time evolution, let us first consider the stress–energy density in the initial state by setting $t=0$.

3.3.1. Casimir energy density of the gapped initial state with boundary. From (57) and (58), the stress–energy density in the initial state is

$$\langle T\,(x)\rangle = \langle \overline{T}\,(x)\rangle = \frac{\pi^2 c}{6\beta^2}\left[3\tanh^2\left(\frac{2\pi\,x}{\beta}\right)-2\right]. \tag{59}$$

The stress–energy density quickly approaches the value $+\frac{\pi^2 c}{6\beta}$ in an infinite system as $x>\beta$. However, as we approach the boundary at $x=0$, the energy density becomes negative, which is similar to the feature of the Casimir effect. Indeed, this negative value near the boundary can be understood based on the following physical picture. The initial state $|\psi_0\rangle = e^{-\frac{\beta}{4}H_{\rm CFT}}|B\rangle\rangle$ has a correlation length $\xi\sim\mathcal{O}(\beta)$. Near the boundary, the system is approximately a CFT living in a finite interval $[0,\xi]$, which gives rise to the negative energy density[8]. This argument is certainly not rigorous, since it is apparent from figure 7 that the negative energy density near the boundary is not uniform.

As a remark, the above point of view was previously considered in [100] in the study of the entanglement Hamiltonian/spectrum of a gapped system, where the entanglement Hamiltonian/spectrum can be considered as that of a CFT living in a length scale of the correlation length ξ with appropriate boundary conditions.

3.3.2. Time evolution. Now let us consider the complex-time evolution of energy density $T_{00}(x,t) = \frac{1}{2\pi}[T(x,t)+\overline{T}(x,t)]$, where $T(x,t)$ and $\overline{T}(x,t)$ are given in (57) and (58), respectively. One can find that $T_{00}(x,t)$ decays to the ground-state value, which is zero, in the long time limit $t\to\infty$.

For a general time t, we plot the averaged energy density in a subregion $[0,l]$ at the end of the system, as shown in figure 8, where the lattice model results and the CFT

[8] One way to understand the CFT behavior in this short-range entangled initial state is to consider the entanglement Hamiltonian (48) for subsystem $[0,l]$ with $l\ll\beta$ at $t=0$. One finds that the (inverse) entanglement temperature is $\beta_E(x) = \overline{\beta}_E(x)\simeq 2\pi\,(l^2-x^2)/2l$, which corresponds to the CFT result.

J. Stat. Mech. (2024) 103103

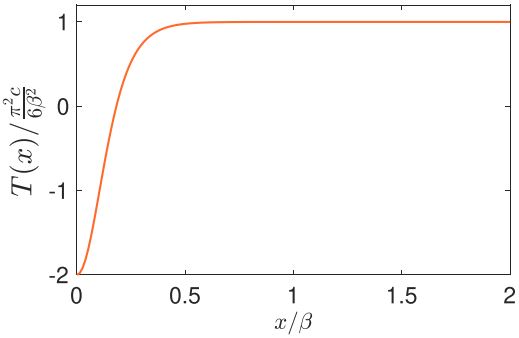

Figure 7. Stress–energy density $\langle T(x)\rangle$ in the initial state $|\psi_0\rangle = e^{-\frac{\beta}{4}H_{\rm CFT}}|B\rangle\rangle$ for a semi-infinite system in $[0,+\infty)$, where the boundary is imposed at $x=0$. For $x>\beta$, $\langle T(x)\rangle$ approaches $\frac{\pi^2 c}{6\beta^2}$, which is the expected value in an infinite system of finite temperature β. The negative value near $x=0$ can be understood based on the Casimir effect.

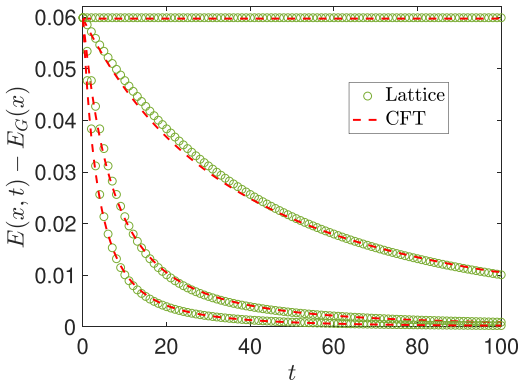

Figure 8. Comparison of complex-time evolution of energy density in lattice and CFT calculations. In the lattice calculation, the energy density is calculated by considering the average $\frac{1}{l}\int_0^l E(x,t)\mathrm{d}x$ in $[0,l]$ with $l=100$ at the end of the system of length $L=800$. From top to bottom, we have $\epsilon=0$, 0.01, 0.05 and 0.1. The fitting parameter in CFT is $\beta=2.94$.

results agree very well[9]. One finds that as we increase ϵ in the complex-time evolution, the (averaged) energy density decays faster in time, as expected.

4. Local quenches with complex metrics

For local quantum quenches in a CFT, there are various setups where the time evolutions are exactly solvable; see, e.g. [47, 101–104]. In this work, we will consider the setup proposed in [47, 101], which we will briefly review as follows.

[9] Note that the Casimir effect which happens in a short length scale $\xi\sim\mathcal{O}(\beta)$ near the boundary is hard to observe in a lattice system, where the energy density fluctuates near the boundary of the lattice. This is why we consider an averaged energy density in the boundary region.

J. Stat. Mech. (2024) 103103

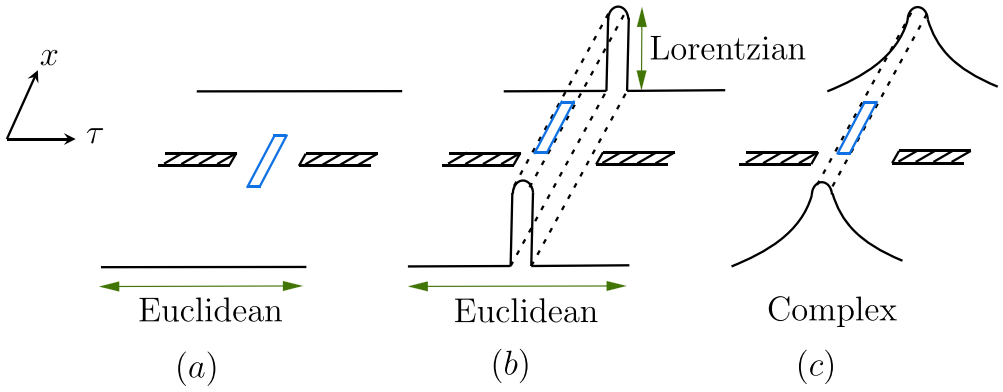

Figure 9. Path integral representation of the reduced density matrix ρ_A after a local quantum quench in a CFT with (a) Euclidean, (b) mixed (partial Euclidean and partial Lorentz), and (c) complex spacetime metrics. The location of the branch cuts (blue lines) corresponds to the subsystem $A=[a,b]$. There are two slits along the imaginary time direction in each configuration, which are used to prepare the initial state in (60).

We consider two CFTs defined on $(-\infty,0)$ and $(0,+\infty)$, with the same conformal boundary conditions imposed at the two ends, respectively. Then, at $t=0$, we join the two ends of the CFTs at $x=0$ suddenly and let the system evolve in time under the uniform CFT Hamiltonian $H_{\rm CFT}$ that is defined over $(-\infty,+\infty)$. Note that the initial state itself is not translationally invariant:

$$|\psi_0\rangle = e^{-\lambda H_{\rm CFT}}\left(|G_L\rangle\otimes|G_R\rangle\right), \quad \lambda\in\mathbb{R}, \tag{60}$$

where $|G_L\rangle$ and $|G_R\rangle$ denote the ground states of the two decoupled CFTs on the left and right sides, respectively, and the factor $e^{-\lambda H_{\rm CFT}}$ is introduced as a regularization. The path integral of the above initial state $|\psi_0\rangle$ is then straightforward: one can introduce a slit that goes from $-i\infty$ to $-i\lambda$ in the imaginary time direction, and then evolve the state from $-i\lambda$ to 0 using a CFT Hamiltonian. Then, we can consider the time evolution of this initial state as well as the corresponding (reduced) density matrix under different spacetime metrics, as shown in figure 9.

Here, we are interested in the complex-time evolution in (6). The time-dependent density matrix we consider here is

$$\rho(t) = e^{-(\lambda+\epsilon t+it)H_{\rm CFT}}\left(|G_L\rangle\otimes|G_R\rangle\right)\left(\langle G_L|\otimes\langle G_R|\right)e^{-(\lambda+\epsilon t-it)H_{\rm CFT}}. \tag{61}$$

To study this density matrix and related physical quantities, one can first consider the two-time density matrix in Euclidean space as follows:

$$\rho(\tau_1,\tau_2) = e^{-(\lambda+\epsilon\tau_1+\tau_2)H_{\rm CFT}}\left(|G_L\rangle\otimes|G_R\rangle\right)\left(\langle G_L|\otimes\langle G_R|\right)e^{-(\lambda+\epsilon\tau_1-\tau_2)H_{\rm CFT}}, \tag{62}$$

J. Stat. Mech. (2024) 103103

based on which one can evaluate $\rho_A(\tau_1,\tau_2)=\mathrm{Tr}_{\overline{A}}\rho(\tau_1,\tau_2)$. Then, in the final step, one can obtain the reduced density matrix $\rho_A(t)$ by taking an analytical continuation $\tau_1\to t$ and $\tau_2\to it$.

4.1. Entanglement Hamiltonian and entanglement spectrum evolution

To study the entanglement Hamiltonian $K_A(t)$ for $A=[0,+\infty)$, let us start from the path integral of the two-time reduced density matrix $\rho_A(\tau_1,\tau_2)$ in the Euclidean space as follows:

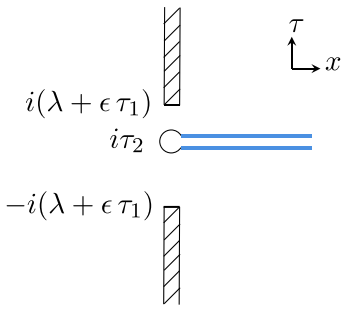

(63)

There are two slits along the imaginary time direction: one is from $-i\infty$ to $-i(\lambda+\epsilon\tau_1)$, and the other is from $i(\lambda+\epsilon\tau_1)$ to $+i\infty$. The branch cut corresponding to subsystem A is along $C=\{i\tau_2+x,x\geqslant 0\}$. A small disk of radius ϵ_0 is removed at the entanglement point $z_0=0+i\tau_2$, with a conformal boundary condition imposed along the boundary.

Next, we consider the conformal mapping:

$$w=f(z)=\log\frac{\sqrt{\left[(\lambda+\epsilon\tau_1)^2-\tau_2^2\right]\cdot\left[(\lambda+\epsilon\tau_1)^2+z^2\right]}-i\tau_2\,z-(\lambda+\epsilon\tau_1)^2}{(\lambda+\epsilon\tau_1)(z-i\tau_2)}, \tag{64}$$

which maps $\rho_A(\tau_1,\tau_2)$ in (63) to a w-cylinder (see, e.g. the right plot in figure 3). The length of this cylinder in the $\mathrm{Im}\,w$ direction is 2π, and the length in the $\mathrm{Re}\,w$ direction is denoted as $W(t)$. Then, the entanglement Hamiltonian corresponds to the generator of translation in the $\mathrm{Im}\,w$ direction of this cylinder. By following the same procedure as in section 2.1, one can obtain

$$\begin{aligned}K_A(t)=&\int_0^\infty\frac{x\sqrt{(x-t)^2+(\lambda+\epsilon t)^2}}{\sqrt{(\lambda+\epsilon t)^2+t^2}}T(x-t)\,\mathrm{d}x\\&+\int_0^\infty\frac{x\sqrt{(x+t)^2+(\lambda+\epsilon t)^2}}{\sqrt{(\lambda+\epsilon t)^2+t^2}}\overline{T}(x+t)\,\mathrm{d}x.\end{aligned} \tag{65}$$

J. Stat. Mech. (2024) 103103

Now let us consider the entanglement temperature as defined in (10). For $\epsilon = 0$ and $t \gg \lambda$, one can find that the entanglement temperature $\beta_E^{-1}(x)$ is low everywhere except near $x = t$:

$$\beta_E(x = t, t) = 2\pi \cdot \frac{\lambda t}{\sqrt{\lambda^2 + t^2}} \simeq 2\pi\lambda. \tag{66}$$

That is, near $x = t$, the entanglement temperature $1/\beta_E(x) \simeq \frac{1}{2\pi\lambda}$ is very high, which means that this region is highly entangled with $\overline{A} = (-\infty, 0)$. In fact, if one studies the entanglement Hamiltonian for $\overline{A}$, one can find $1/\overline{\beta}_E(x = -t, t) \simeq \frac{1}{2\pi\lambda}$, which indicates that there is a maximal entanglement between the regions near $x = -t$ and $x = t$. This agrees with the quasi-particle picture as studied in [47, 101, 102, 105, 106].

Now, let us consider the complex-time evolution with $\epsilon > 0$. For the entanglement Hamiltonian of $A = [0, +\infty)$, one can find that the entanglement temperature at $x = t$ becomes

$$\beta_E(x = t, t) = 2\pi \frac{(\lambda + \epsilon t)\, t}{\sqrt{(\lambda + \epsilon t)^2 + t^2}}. \tag{67}$$

In the long time limit $t \gg \lambda/\epsilon$, one can find

$$\beta_E(x = t, t) \propto 2\pi t. \tag{68}$$

That is, as t grows, the entanglement temperature $1/\beta_E(x) \propto \frac{1}{2\pi t}$ will decay to zero in time. In other words, the entanglement between the two regions near $x = -t$ and $x = t$ keeps decreasing in time due to the damping effect.

– *Time evolution of entanglement spectrum:*

Next, let us consider the time evolution of the entanglement spectrum. Similar to the analysis in section 2, the spacing of the entanglement spectrum is determined by (31). Based on the conformal map in (64), one can find

$$W(t) = \log \frac{2\left[t^2 + (\lambda + \epsilon t)^2\right]}{\epsilon_0 (\lambda + \epsilon t)} + \mathcal{O}(\epsilon_0). \tag{69}$$

In a real-time evolution ($\epsilon = 0$), one can find that $W(t) \simeq 2\log t$ for $t \gg \lambda$. In a complex-time evolution ($\epsilon > 0$), one can find that $W(t) \simeq \log t$ for $t \gg \lambda/\epsilon$. Then, from (31), the long time evolution of the entanglement spectrum has the following scaling behavior:

$$\begin{cases} \text{Spacing of entanglement spectrum} \sim \frac{1}{2\log t}, & \text{real time evolution}\,(\epsilon = 0), \\ \text{Spacing of entanglement spectrum} \sim \frac{1}{\log t}, & \text{complex time evolution}\,(\epsilon > 0). \end{cases} \tag{70}$$

Note that there is a factor 2 difference between the real- and complex-time evolutions.

J. Stat. Mech. (2024) 103103

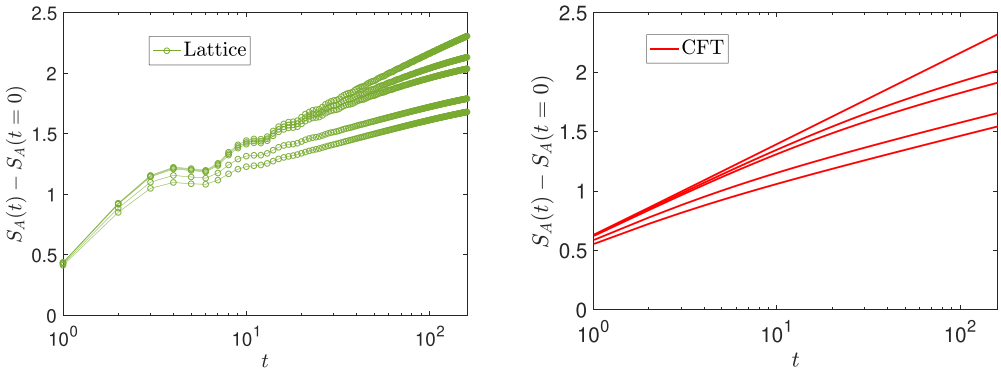

Figure 10. Comparison of complex-time evolution of entanglement entropy $S_A(t)$ after a local quench in a lattice system (left) and in CFT calculation (right). The lattice system is defined on $[0,L]=[0,800]$, and $A=[0,400]$. The CFT result is plotted according to (71), where we choose $\lambda=0.15$. Note that ϵ_0 is canceled out in $S_A(t)-S_A(t=0)$. From top to bottom, we choose $\epsilon=0$, 0.005, 0.01, 0.05 and 0.1.

4.2. Entanglement entropy evolution

The entanglement entropy evolution is related to $W(t)$ in (69) via the same formula as in (38). It is found that

$$S_A(t)=\frac{c}{6}\log\frac{2\left[t^2+(\lambda+\epsilon t)^2\right]}{\epsilon_0(\lambda+\epsilon t)}+\log g_a+\log g_b+\mathcal{O}(\epsilon_0). \tag{71}$$

A plot of $S_A(t)$ from both the lattice model calculation and the CFT calculation can be found in figure 10. It is apparent that the complex time ($\epsilon>0$) will suppress the entanglement entropy evolution in time. In particular, one can find the following simple scaling behavior in the long time limit:

$$\begin{cases} S_A(t)\simeq\frac{c}{3}\log t, & t\gg\lambda \text{in real time evolution}\,(\epsilon=0),\\ S_A(t)\simeq\frac{c}{6}\log t, & t\gg\lambda/\epsilon \text{in complex time evolution}\,(\epsilon>0). \end{cases} \tag{72}$$

Similar to the entanglement spectrum evolution in (70), here we have a factor 2 difference in the real- and complex-time evolutions of $S_A(t)$.

4.3. Energy density evolution

In real time, the energy density evolution after a local quench has been studied [106, 107]. Since the initial state in (60) is not translation invariant, one will observe a flow of energy density emitted from $x=0$ where we join the two CFTs after the quench. Here, we are interested in the complex-time evolution.

J. Stat. Mech. (2024) 103103

We consider the one-point function $\langle T(z)\rangle$ by inserting the holomorphic stress–energy tensor operator at $z=x+i\tau_2$ in the configuration in (63) (with the branch cuts removed). By using the conformal mapping

$$w=f(z)=\frac{1}{\lambda+\epsilon\tau_1}\left(z+\sqrt{z^2+(\lambda+\epsilon\tau_1)^2}\right), \tag{73}$$

one can map (63) to an RHP. Since $\langle T(w)\rangle_{\rm RHP}=0$, one can obtain

$$\langle T(x,t)\rangle=-\frac{c}{12}\{w,z\}=\frac{c}{8}\cdot\frac{(\lambda+\epsilon t)^2}{\left[(x-t)^2+(\lambda+\epsilon t)^2\right]^2}, \tag{74}$$

where in the last step we have taken the analytical continuation $\tau_1\to t$ and $\tau_2\to it$. Similarly, one can obtain

$$\langle\overline{T}(x,t)\rangle=\frac{c}{8}\cdot\frac{(\lambda+\epsilon t)^2}{\left[(x+t)^2+(\lambda+\epsilon t)^2\right]^2}. \tag{75}$$

Therefore, the time evolution of the energy density $\langle T_{00}(x,t)\rangle=\frac{1}{2\pi}\left[\langle T(x,t)\rangle+\langle\overline{T}(x,t)\rangle\right]$ is

$$\langle T_{00}(x,t)\rangle=\frac{c}{16\pi}\left(\frac{(\lambda+\epsilon t)^2}{\left[(x-t)^2+(\lambda+\epsilon t)^2\right]^2}+\frac{(\lambda+\epsilon t)^2}{\left[(x+t)^2+(\lambda+\epsilon t)^2\right]^2}\right). \tag{76}$$

For $\epsilon=0$, it reproduces the real-time evolution result [106]. In particular, at $x=\pm t$, one can observe two peaks in the energy density with

$$\langle T_{00}(x=\pm t,t)\rangle\simeq\frac{c}{16\pi}\cdot\frac{1}{\lambda^2}. \tag{77}$$

This is in comparison with the regions $|x\pm t|\gg\lambda$, where $T_{00}(x,t)\simeq 0$. This feature of propagating energy density peaks can be observed in both the CFT and lattice calculations, as shown in figure 11. It has been shown that these two peaks, which are emitted from $x=0$, are strongly entangled with each other [102, 105, 106]; see also a related discussion on the entanglement temperature near (66).

Now, by considering a complex-time evolution, one can still observe two peaks in the energy density evolution. The difference is that these propagating excitations die out in time. More explicitly, the peaks at $x=\pm t$ are suppressed in time as

$$\langle T_{00}(x=\pm t,t)\rangle\simeq\frac{c}{16\pi}\cdot\frac{1}{(\lambda+\epsilon t)^2}, \tag{78}$$

which decays to zero as a function of $1/t^2$ in the long time limit. A sample plot of $\langle T_{00}(x,t)\rangle$ for both the lattice model calculations and the CFT calculations can be

J. Stat. Mech. (2024) 103103

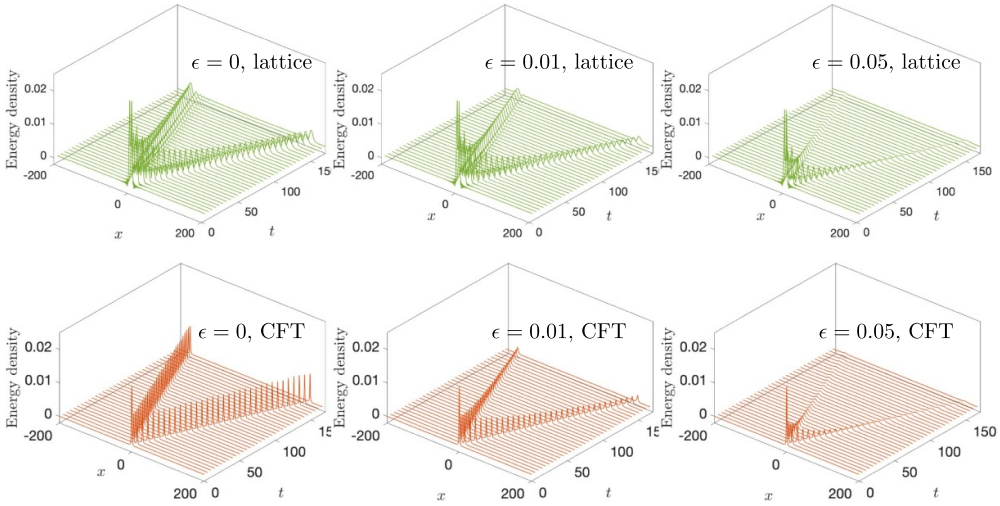

Figure 11. Complex-time evolution of energy density $\langle T_{00}(x,t)\rangle$ after a local quantum quench in the free-fermion lattice (top) and CFT (bottom) calculations, with $\epsilon = 0$, 0.01 and 0.05, respectively. In the CFT calculation, we take $\lambda = 1.5$ in (76).

found in figure 11, where one can clearly see that the energy density peaks emitted from $x = 0$ gradually die out in time for $\epsilon > 0$.

5. Periodically driven critical systems with complex metrics: competition between driving and damping

In the previous sections on quantum quenches, we have seen that complex-time evolutions give rise to a damping effect in the non-equilibrium dynamics. Note that in a quantum quench the excitations are injected *only* at $t = 0$, and then there is no further driving. Then, as time evolves, the system will gradually decay to the ground state due to the damping effect.

In this section, we are interested in the case of time-dependent drivings, and in particular the competition between driving and damping. The setup we consider here is the so-called Floquet CFT, the real-time evolution of which is exactly solvable [48]. See some recent progress along this direction in quantum field theory [48–71] and the holographic dual [72–80]. The basic idea is to drive the system with time-dependent Hamiltonians

$$H(t) = \int_0^L f(x,t)\, T_{00}(x)\, \mathrm{d}x, \tag{79}$$

where $T_{00}(x)$ is the energy density in a CFT, and $f(x,t)$ is a real-value function. For a fixed time t, the effect of $f(x,t)$ is to deform the Hamiltonian density in space. The effect of such time-dependent driving is to perform a conformal transformation on operators, which is the underlying reason why this setup is exactly solvable. One interesting feature

J. Stat. Mech. (2024) 103103

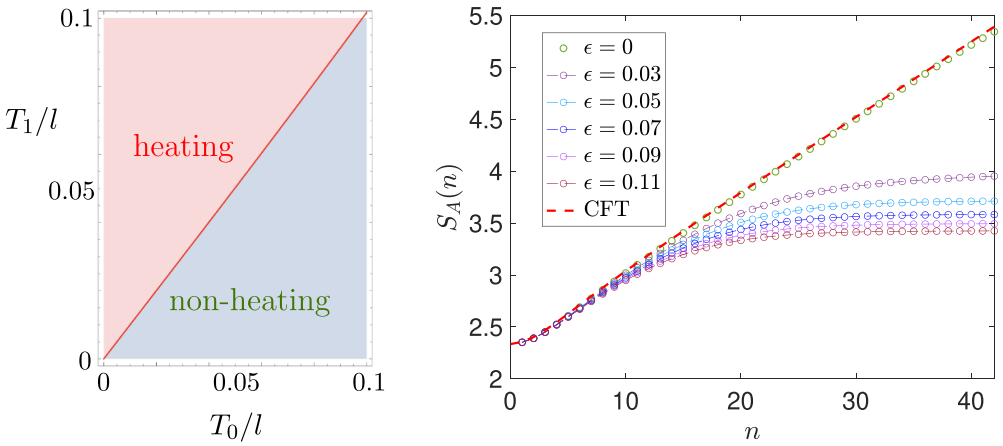

Figure 12. Left: phase diagram of the Floquet CFT in a real-time evolution in (80). Right: complex-time evolution of entanglement entropy $S_A(n)$ during a periodic driving, where n is the driving period in (82) and the driving Hamiltonians are chosen in (81). We choose $L = 2l = 400$ with periodical boundary conditions, and the subsystem is $A = [0, L/2]$. The driving parameters are chosen as $T_0/l = 1/50$ and $T_1/l = 1/25$ in (82), which is in the heating phase of a Floquet CFT if $\epsilon = 0$. Dashed red line corresponds to the CFT result in the real-time evolution, which can be obtained based on the approach in [48]. For $\epsilon > 0$, the entanglement entropy will reach a steady value, which decreases as one increases ϵ.

in this setup is that there can be different phases, including the heating and non-heating phases with a phase transition, depending on the driving parameters [48]. In particular, in the heating phase, the total energy of the system grows exponentially in time, and the entanglement entropy grows linearly in time. The energy and entanglement growths also exhibit interesting spatial features: the absorbed energy during the driving is mainly accumulated at certain hot spots (see, e.g. figure 15 in a later discussion), and the entanglement entropy is mainly contributed by the entanglement between excitations localized at the neighboring hot spots [50].

Now let us consider a concrete and minimal setup of Floquet CFT. We start from the ground state $|G\rangle$ of a uniform CFT Hamiltonian H_0, and evolve the state $|\psi_0\rangle = |G\rangle$ with periodically changing Hamiltonians as follows:

$$\begin{cases} H_0 = \int_0^L T_{00}(x)dx, \\ H_1 = \int_0^L \cos\left(\dfrac{2\pi x}{l}\right) T_{00}(x)\, dx \end{cases} \qquad \begin{array}{l} H_1 \\ H_0 \end{array} \quad \cdots \quad \text{time} \tag{80}$$

That is, we evolve the system with Hamiltonians H_0 and H_1 for times T_0 and T_1, respectively, in a periodic way (see also equation (7)). The corresponding non-equilibrium phase diagram is shown in figure 12.

J. Stat. Mech. (2024) 103103

Now, by introducing a complex-time evolution in the heating phase, there will be a competition between the driving and damping. Although the real-time evolution is exactly solvable, unfortunately we do not know how to analytically solve the *complex-time* evolution in a Floquet CFT with allowable complex spacetime metrics [1]. Therefore, in the following discussions, we will rely on numerical calculations based on a free-fermion lattice model to study the complex-time evolution. As a remark, in the real-time evolution, it has been shown that such free-fermion model calculations agree with the CFT calculations in a remarkable way [49, 60].

To be concrete, we consider the complex-time evolution with the following two driving Hamiltonians on a lattice:

$$\begin{cases} H_0 &= -\frac{1}{2}\sum_{i=1}^{L} c_i^\dagger c_{i+1} + h.c., \\ H_1 &= -\frac{1}{2}\sum_{i=1}^{L} f_j\, c_i^\dagger c_{i+1} + h.c., \end{cases} \tag{81}$$

where c_i and $c_i^\dagger$ are fermionic annihilation and creation operators that satisfy the anti-commutation relations $\{c_i, c_j\} = \{c_i^\dagger, c_j^\dagger\} = 0$, and $\{c_i, c_j^\dagger\} = \delta_{ij}$. Here, we choose f_j as the discrete version of $f(x) = \cos\left(\frac{2\pi x}{l}\right)$ in (80), with $L = 2l$. That is, H_0 is a free-fermion lattice with uniform hopping, while the Hamiltonian density in H_1 is deformed by f_j. The initial state is chosen as the ground state $|G\rangle$ of H_0 with a half filling. This setup of driving in a real-time evolution is exactly the same as that considered in [64]. Now, the complex-time evolution we consider is

$$|\psi(n)\rangle = \left(e^{-i(1-i\epsilon)H_0 T_0} e^{-iH_1 T_1}\right)^n |G\rangle, \tag{82}$$

where we introduce the complex time only during the driving by H_0. The motivation is that the time-dependent driving can lead to a heating phase [48], where the system keeps absorbing energy and evolves to a highly excited state of H_0 in time. At the same time, the factor $e^{-\epsilon H_0 T_0}$ in the driving has a damping effect, which tends to evolve the system to the ground state $|G\rangle$ of H_0. When both driving and damping are present, it is expected that the system will reach a steady state.

5.1. Entanglement entropy and entanglement spectrum evolution

To observe the competition between driving and damping, we first study the complex-time evolution of entanglement entropy. As shown in figure 12, by first setting $\epsilon = 0$, we tune the driving parameters T_0 and T_1 in (82) to the heating phase in a Floquet CFT [48], where the entanglement entropy of a subsystem grows linearly in time. By turning on the complex time with $\epsilon > 0$ in (82), one can find that the entanglement entropy reaches a steady state value. As one increases ϵ, the steady value decreases—this is as expected, since a larger ϵ corresponds to a larger damping rate to the ground state. Next, to see the spatial features of the entanglement, we check the entanglement entropy density $S_A(x,n)$ for a small subsystem $A = [x - l_A/2, x + l_A/2]$. As shown in figure 13, in a real-time evolution ($\epsilon = 0$), the entanglement entropy density $S_A(x,n)$ form peaks in the real space, and the peaks grow linearly in time [50]. By turning on the complex-time evolution with $\epsilon > 0$, one can still observe the peaks of entanglement

J. Stat. Mech. (2024) 103103

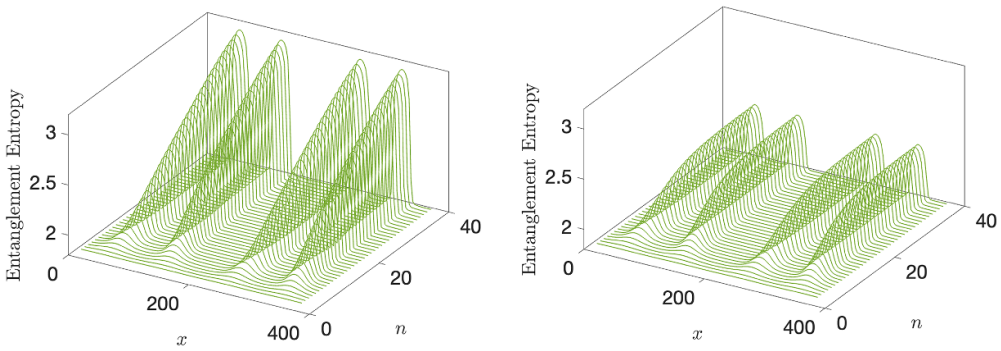

Figure 13. Complex-time evolution of entanglement entropy density $S_A(x,n)$ for subsystem $A=[x-l_A/2,x+l_A/2]$ during a periodic driving. We choose $L=400$ with periodical boundary conditions, and the length of the subsystem is $l_A=30$. The driving parameters are the same as those in figure 12. In a real-time evolution with $\epsilon=0$ (left), the entanglement entropy density forms peaks in the real space, and these peaks grow linearly in time. In a complex-time evolution with $\epsilon=0.11$ (right), the peaks in $S_A(x,n)$ form at the same locations, grow first and then saturate at a steady value.

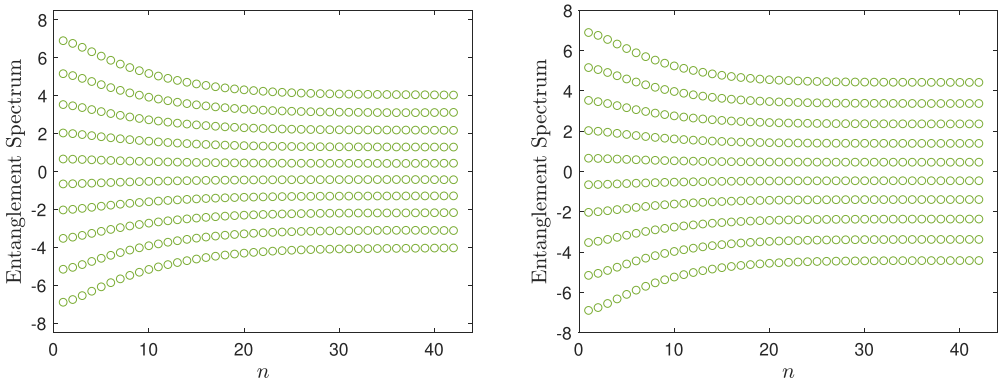

Figure 14. Complex-time evolution of entanglement spectrum for subsystem $A=[0,L/2]$. The parameters are the same as those in figure 12, with $\epsilon=0.05$ (left) and $\epsilon=0.11$ (right). As ϵ increases, the steady value of spacing in the entanglement spectrum increases, which results in a smaller entanglement entropy in figure 12.

entropy density at the same locations. These peaks grow in time at the beginning and then saturate at a steady value that depends on the concrete choice of ϵ.

We further examine the complex-time evolution of the entanglement spectrum in the subsystem $A=[0,L/2]$. In a real-time evolution, since the entanglement entropy grows linearly in time, the spacing of the entanglement spectrum will keep decreasing in time. In a complex-time evolution, however, the spacing of the entanglement spectrum reaches a steady value, as seen in figure 14. This steady value will increase as we increase ϵ, which results in a decreasing entanglement entropy. This is consistent with the result in the time evolution of entanglement entropy in figure 12.

J. Stat. Mech. (2024) 103103

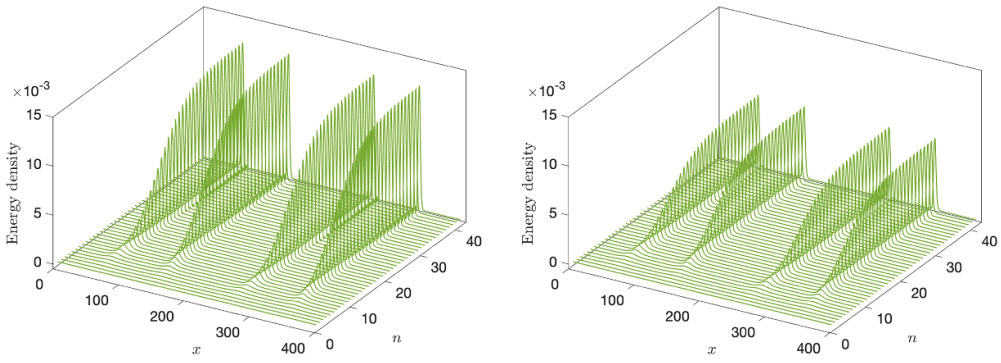

Figure 15. Complex-time evolution of energy density in a Floquet CFT with $L = 400$. The driving parameters are the same as those in figure 12, with $\epsilon = 0.07$ (left) and $\epsilon = 0.11$ (right). A larger ϵ leads to a smaller steady value of the energy density at the hot spots.

5.2. Energy density evolution

Finally, we examine the time evolution of the energy density. In a real-time evolution in the heating phase, it is known that the total energy will grow exponentially in time, and the absorbed energy is mainly accumulated at certain hot spots in the real space [50, 52, 64]. In a complex-time evolution, we find that the absorbed energy is still accumulated at such hot spots (see figure 15), but will reach a steady value, which is similar to the feature of the entanglement entropy/spectrum evolution. In addition, as we increase ϵ, the steady value of the energy density at the hot spots will decrease, as expected.

In short, based on a numerical study of the entanglement entropy and energy density evolution in a free-fermion lattice model with complex spacetime metrics, one finds that the competition between the driving and damping leads to a steady state, where the patterns of entanglement and energy density are inherited from those in a Floquet CFT in a real-time evolution. It is an interesting future problem to give an analytical study of the features observed in the above numerical calculations.

6. Discussion and conclusion

The method in this work can be generalized to other interesting cases. For example, one can consider the following complex-time evolution:[10]

$$|\psi(t)\rangle = e^{-iH_{\rm CFT}(t-i\epsilon t^{\alpha})}|\psi_0\rangle, \quad \epsilon \geqslant 0, \alpha \in \mathbb{R}. \tag{83}$$

In comparison with (6), here we have replaced ϵt with ϵt^{α}. The entanglement Hamiltonian and other quantities can be studied in the same way as we did in the main text for each setup. For example, for the global quantum quench as considered in section 2, the time evolution of entanglement entropy can be obtained from (38)

[10] We thank Shinsei Ryu for asking this question.

J. Stat. Mech. (2024) 103103

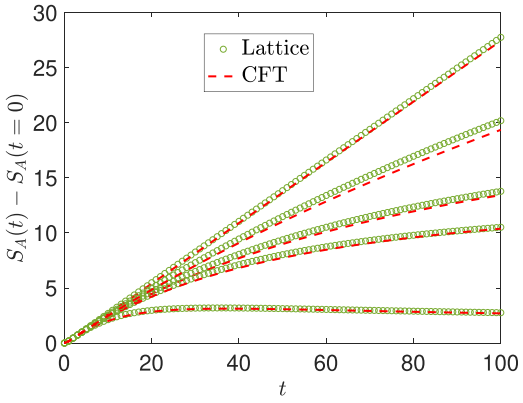

Figure 16. Comparison of complex-time evolution of entanglement entropy $S_A(t)$ after a global quench according to (83) in a free-fermion lattice system and CFT calculations. The lattice system is defined on $[0, L] = [0, 800]$, and the subsystem is $A = [0, 400]$. We choose $\epsilon = 0.01$, and $\alpha = 1.5$, 1.1, 1 and 0.8 from bottom to top. For the top curve, it is a real-time evolution with $\epsilon = 0$. The CFT result is plotted according to (38) and (35) by replacing ϵt with ϵt^{α}. The fitting parameters are $\beta = 3.75$ and $\epsilon_0 = 0.1$.

and (35) by simply replacing ϵt with ϵt^{α}. See figure 16 for a comparison of lattice and CFT calculations for this case.

Now let us briefly conclude this work and mention some future problems.

In this work, we have studied the effect of allowable complex spacetime metrics (as recently proposed in [1] and [4]) on global/local quantum quench dynamics as well as time-dependent drivings in $(1+1)$-dimensional CFTs. For quantum quenches, the time evolution of various physical quantities can be analytically solved at an arbitrary time. The non-equilibrium dynamics in a complex-time evolution show universal features that are qualitatively different from those in a real-time evolution; see, e.g. (13)–(15) for a comparison of the entanglement entropy evolution. Physically, this qualitative difference is caused by the damping effect introduced by a complex time. We further investigate the competition between the damping effect and external driving by studying the recently proposed Floquet CFT [48] in a complex spacetime metric. To our knowledge, this Floquet CFT setup, although analytically solvable in the real-time evolution, cannot be solved analytically in the allowable complex spacetime metrics. By performing a numerical study on a lattice model, it is found that the competition between driving and damping can lead to a steady state with interesting patterns for the entanglement and energy density distribution.

Finally, we want to point out several interesting future problems:

The complex-time evolution considered in this work is generated by CFT Hamiltonians. For many interesting cases in non-unitary dynamics (see, e.g. some recent works [23–34]), the corresponding Hamiltonians in the non-unitary time evolutions are not exactly CFT Hamiltonians. It will be interesting to generalize our discussion in this work to the following Hamiltonians with a complex-time evolution: $H_{\rm CFT} \to H_{\rm CFT} + \sum_i \lambda_i \int \Phi_i(x)\,{\rm d}x$, where $\{\Phi_i\}$ could be irrelevant, marginal or relevant operators depending on the concrete physical problems, and $\{\lambda_i\}$ are real numbers.

J. Stat. Mech. (2024) 103103

A good understanding of this generalization may bring some insights to those problems in open quantum systems.

Another interesting future problem is to give an analytical study of the time-dependent driven CFTs with allowable complex spacetime metrics. From the numerical study on a free-fermion lattice model in section 5, we have seen that the competition between driving and damping results in a steady state with interesting entanglement features. It will be interesting to understand this steady state for a general CFT in an analytical way.

Note added: During the preparation of this draft, I was aware of [108], which studied the non-unitary time evolution in 2D CFTs in a different setup. Aside from the setup, the spacetime metrics considered therein are partially Lorentz and partially Euclidean, while in this work we consider complex metrics.

Note added 2: We thank the authors of [109] for letting us know that they did a similar analysis on the complex-time evolution of entanglement entropy after a global quantum quench, which has a partial overlap with our results in section 3.2.

Acknowledgments

The author thanks for the interesting discussions with Po-Yao Chang, Birgit Kaufmann, Ching Hua Lee, Shinsei Ryu, Qicheng Tang and Ashvin Vishwanath. This work is in part supported by the Simons Collaboration on Ultra-Quantum Matter, which is a grant from the Simons Foundation (618615, 651440). This work is also supported by a startup at Georgia Tech.

Appendix . Details of the free-fermion lattice with a complex-time evolution

The complex-time evolution of a free-fermion lattice model can be studied by a straightforward generalization of the real-time evolution; see, e.g. the detailed study in [36]. Thanks to Wick's theorem, to study the entanglement entropy/spectrum in a free-fermion lattice, it is enough to know the time-dependent two-point functions [110].

We consider a free-fermion Hamiltonian of the general form $H=\sum_{i,j=1}^{L}H_{ij}\,c_i^\dagger c_j$, where L is the total number of lattice sites. Here, c_i and $c_i^\dagger$ are fermionic annihilation and creation operators that satisfy the anticommutation relations $\{c_i,c_j\}=\{c_i^\dagger,c_j^\dagger\}=0$, and $\{c_i,c_j^\dagger\}=\delta_{ij}$. Note that although we are interested in the complex-time evolution, the Hamiltonian we consider here is always Hermitian. The Hamiltonian can be diagonalized by a unitary matrix with $c_i=\sum_j U_{ij}\gamma_j$ such that $H=\sum_{i=1}^{L}E_i\,\gamma_i^\dagger\gamma_i$. Then, the ground state with the lowest N energy levels filled is

$$|G\rangle=\prod_{i=1}^{N}\gamma_i^\dagger|\mathrm{vac}\rangle=\prod_{i=1}^{N}\left(\sum_{j=1}^{L}c_j^\dagger U_{ji}\right)|\mathrm{vac}\rangle. \tag{84}$$

For later convenience, we denote U^f as the first N columns of the unitary matrix U. That is, U^f is an L by N matrix. One can rewrite the ground state as $|G\rangle = \prod_{i=1}^{N}\left(\sum_{j=1}^{L} c_j^\dagger U^f_{ji}\right)|\text{vac}\rangle$.

Now we consider a quantum quench after a complex-time evolution: $|\psi_1(t)\rangle = e^{-i(1-i\epsilon)H_1 t}|G\rangle$. Let us denote this state as $|\psi_1(t)\rangle = e^{-z_1 H_1}|G\rangle$, where we have defined $z_1 := i(1-i\epsilon)t$. By considering the general formula

$$e^{\sum_{i,j} P_{ij} c_i^\dagger c_j}\, c_l^\dagger\, e^{-\sum_{i,j} P_{ij} c_i^\dagger c_j} = \sum_m \left(e^P\right)_{ml} c_m^\dagger, \tag{85}$$

one can find that

$$|\psi_1(t)\rangle = e^{-z_1 H_1}|G\rangle = \prod_{i=1}^{N}\left(\sum_{j=1}^{L} c_j^\dagger \left[e^{-z_1 H_1} U^f\right]_{ji}\right)|\text{vac}\rangle =: \prod_{i=1}^{N}\left(\sum_{j=1}^{L} c_j^\dagger \widetilde{U}_{ji}\right)|\text{vac}\rangle. \tag{86}$$

Note that $\widetilde{U} = e^{-z_1 H_1} U^f$ is an L by N matrix. The first thing to notice is that even for a normalized initial state $\langle G|G\rangle = 1$, we no longer have $\langle\psi_1(t)|\psi_1(t)\rangle = 1$ after a non-unitary time evolution. Instead, we have

$$\langle\psi_1(t)|\psi_1(t)\rangle = \det\left[\widetilde{U}^\dagger \widetilde{U}\right]. \tag{87}$$

Next, based on (86), it is straightforward to check that

$$\langle\psi_1(t)|c_m^\dagger c_n|\psi_1(t)\rangle = \left[\widetilde{U}\,\text{adj}\left(\widetilde{U}^\dagger\widetilde{U}\right)\widetilde{U}^\dagger\right]_{nm} \tag{88}$$

where $\text{adj}(M)$ denotes the adjugate of the matrix M. Then, based on (87) and (88), one finds that the two-point function after normalizing the state is

$$\frac{\langle\psi_1(t)|c_m^\dagger c_n|\psi_1(t)\rangle}{\langle\psi_1(t)|\psi_1(t)\rangle} = \left[\widetilde{U}\left(\widetilde{U}^\dagger\widetilde{U}\right)^{-1}\widetilde{U}^\dagger\right]_{nm}, \tag{89}$$

where M^{-1} is the inverse of M with $M^{-1} = \text{adj}(M)/\det(M)$. Based on this correlation matrix, one can follow the procedure in [110] to further obtain the entanglement spectrum and entanglement entropy.

The above discussion can be straightforwardly generalized to a time-dependent driving case, e.g. the periodically driven case in section 5, by simply re-defining the matrix $\widetilde{U}$ in (86) as

$$\widetilde{U} = \left(e^{-z_n H_n}\cdots e^{-z_1 H_1}\right) U^f, \tag{90}$$

where it is reminded that U^f is the first N columns of the unitary matrix U in (84).

J. Stat. Mech. (2024) 103103

Next, let us briefly introduce the lattice model we used to compare with the CFT calculation in the main text. In the global quench, the initial state $|\psi_0\rangle$ is prepared as the ground state of the following gapped Hamiltonian:

$$H_0 = -\frac{1}{2}\sum_i c_i^\dagger c_{i+1} + h.c. + m\sum_i (-1)^i\, c_i^\dagger c_i. \tag{91}$$

Here, the mass term $m \in \mathbb{R}$ determines the size of gap in the energy spectrum. Then at $t=0$, we evolve the initial state as $|\psi_1(t)\rangle = e^{-iH_1(1-i\epsilon)t}|\psi_0\rangle$, where H_1 is the critical Hamiltonian by setting $m=0$ in H_0, i.e.

$$H_1 = -\frac{1}{2}\sum_i c_i^\dagger c_{i+1} + h.c. \tag{92}$$

In the local quench, the initial state $|\psi_0\rangle$ is considered as the ground state of two decoupled fermion chains as follows:

$$H_0 = -\frac{1}{2}\sum_{i=0}^{L/2-1} c_i^\dagger c_{i+1} - \frac{1}{2}\sum_{i=L/2}^{L-1} c_i^\dagger c_{i+1} + h.c. \tag{93}$$

Then, at $t=0$, we evolve the initial state with the Hamiltonian H_1 in (92), i.e. we connect the two ends of the free-fermion chains in (93). The time-dependent state is $|\psi_1(t)\rangle = e^{-iH_1(1-i\epsilon)t}|\psi_0\rangle$.

References

[1] Kontsevich M and Segal G 2021 Wick rotation and the positivity of energy in quantum field theory (arXiv:2105.10161)

[2] Streater R F and Wightman A S 2000 *PCT, Spin and Statistics and all That* vol 30 (Princeton University Press)

[3] Louko J and Sorkin R D 1997 Complex actions in two-dimensional topology change *Class. Quantum Grav.* **14** 179

[4] Witten E 2021 A note on complex spacetime metrics (arXiv:2111.06514)

[5] Bondarenko S 2022 Dynamical signature: complex manifolds, gauge fields and non-flat tangent space *Universe* **8** 497

[6] Lehners J-L 2022 Allowable complex metrics in minisuperspace quantum cosmology *Phys. Rev.* D **105** 026022

[7] Jonas C, Lehners J-L and Quintin J 2022 Uses of complex metrics in cosmology (arXiv:2205.15332)

[8] Visser M 2022 Feynman's $i\epsilon$ prescription, almost real spacetimes and acceptable complex spacetimes *J. High Energy Phys.* JHEP08(2022)129

[9] Loges G J, Shiu G and Sudhir N 2022 Complex saddles and Euclidean wormholes in the Lorentzian path integral *J. High Energy Phys.* JHEP08(2022)064

[10] Briscese F 2022 Note on complex metrics, complex time and periodic universes *Phys. Rev.* D **105** 126028

[11] Hertog T, Janssen O and Karlsson J 2023 Kontsevich-Segal criterion in the no-boundary state constrains inflation *Phys. Rev. Lett.* **131** 191501

[12] Dong X, Lewkowycz A and Rangamani M 2016 Deriving covariant holographic entanglement *J. High Energy Phys.* JHEP11(2016)028

[13] Marolf D and Maxfield H 2021 Observations of Hawking radiation: the page curve and baby universes *J. High Energy Phys.* JHEP04(2021)272

[14] Colin-Ellerin S, Dong X, Marolf D, Rangamani M and Wang Z 2021 Real-time gravitational replicas: formalism and a variational principle *J. High Energy Phys.* JHEP05(2021)117

J. Stat. Mech. (2024) 103103

[15] Skinner B, Ruhman J and Nahum A 2019 Measurement-induced phase transitions in the dynamics of entanglement *Phys. Rev.* X **9** 031009
[16] Li Y, Chen X and Fisher M P A 2018 Quantum Zeno effect and the many-body entanglement transition *Phys. Rev.* B **98** 205136
[17] Bao Y, Choi S and Altman E 2020 Theory of the phase transition in random unitary circuits with measurements *Phys. Rev.* B **101** 104301
[18] Jian C-M, You Y-Z, Vasseur R and Ludwig A W W 2020 Measurement-induced criticality in random quantum circuits *Phys. Rev.* B **101** 104302
[19] Tantivasadakarn N, Thorngren R, Vishwanath A and Verresen R 2024 Long-range entanglement from measuring symmetry-protected topological phases *Phys. Rev.* X **14** 021040
[20] Lu T-C, Lessa L A, Kim I H and Hsieh T H 2022 Measurement as a shortcut to long-range entangled quantum matter *PRX Quantum* **3** 040337
[21] Tantivasadakarn N, Vishwanath A and Verresen R 2023 Hierarchy of topological order from finite-depth unitaries, measurement and feedforward *PRX Quantum* **4** 020339
[22] Zhu G-Y, Tantivasadakarn N, Vishwanath A, Trebst S and Verresen R 2023 Nishimori's cat: stable long-range entanglement from finite-depth unitaries and weak measurements *Phys. Rev. Lett.* **131** 200201
[23] Garratt S J, Weinstein Z and Altman E 2023 Measurements conspire nonlocally to restructure critical quantum states *Phys. Rev.* X **13** 021026
[24] Weinstein Z, Sajith R, Altman E and Garratt S J 2023 Nonlocality and entanglement in measured critical quantum Ising chains *Phys. Rev.* B **107** 245132
[25] Yang Z, Mao D and Jian C-M 2023 Entanglement in a one-dimensional critical state after measurements *Phys. Rev.* B **108** 165120
[26] Sun X, Yao H and Jian S-K 2023 New critical states induced by measurement (arXiv:2301.11337)
[27] Murciano S, Sala P, Liu Y, Mong R S K, Alicea J and Ising Quantum Criticality M-A 2023 *Phys. Rev.* X **13** 041042
[28] Sala P, Murciano S, Liu Y and Alicea J 2024 Quantum criticality under imperfect teleportation (arXiv:2403.04843)
[29] Granet E, Zhang C and Dreyer H 2022 Volume-law to area-law entanglement transition in a non-unitary periodic Gaussian circuit (arXiv:2212.10584)
[30] Chen X, Li Y, Fisher M P A and Lucas A 2020 Emergent conformal symmetry in nonunitary random dynamics of free fermions *Phys. Rev. Res.* **2** 033017
[31] Turkeshi X and Schiró M 2023 Entanglement and correlation spreading in non-Hermitian spin chains *Phys. Rev.* B **107** L020403
[32] Tang Q, Chen X and Zhu W 2021 Quantum criticality in the nonunitary dynamics of (2 +1)-dimensional free fermions *Phys. Rev.* B **103** 174303
[33] Milekhin A and Popov F K 2022 Measurement-induced phase transition in teleportation and wormholes (arXiv:2210.03083)
[34] Zerba C and Silva A 2023 Measurement phase transitions in the no-click limit as quantum phase transitions of a non-hermitean vacuum *SciPost Phys. Core* **6** 051
[35] Grundner M, Westhoff P, Kugler F B, Parcollet O and Schollwöck U 2024 Complex time evolution in tensor networks and time-dependent Green's functions *Phys. Rev.* B **109** 155124
[36] Shirakawa T, Seki K and Yunoki S 2021 Discretized quantum adiabatic process for free fermions and comparison with the imaginary-time evolution *Phys. Rev. Res.* **3** 013004
[37] Yeter-Aydeniz K, Moschandreou E and Siopsis G 2022 Quantum imaginary-time evolution algorithm for quantum field theories with continuous variables *Phys. Rev.* A **105** 012412
[38] Prosen T 2008 Third quantization: a general method to solve master equations for quadratic open Fermi systems *New J. Phys.* **10** 043026
[39] Prosen T 2010 Spectral theorem for the Lindblad equation for quadratic open fermionic systems *J. Stat. Mech.* 07020
[40] Horstmann B, Cirac J I and Giedke G 2013 Noise-driven dynamics and phase transitions in fermionic systems *Phys. Rev.* A **87** 012108
[41] Medvedyeva M V, Essler F H L and Prosen T 2016 Exact bethe ansatz spectrum of a tight-binding chain with dephasing noise *Phys. Rev. Lett.* **117** 137202
[42] Rowlands D A and Lamacraft A 2018 Noisy Spins and the Richardson-Gaudin model *Phys. Rev. Lett.* **120** 090401
[43] Shibata N and Katsura H 2019 Dissipative quantum Ising chain as a non-Hermitian Ashkin-Teller model *Phys. Rev.* B **99** 224432

J. Stat. Mech. (2024) 103103

[44] Ziolkowska A A and Essler F 2020 Yang-Baxter integrable Lindblad equations *SciPost Phys.* **8** 044
[45] Robertson J and Essler F H L 2021 Exact solution of a quantum asymmetric exclusion process with particle creation and annihilation *J. Stat. Mech.* 103102
[46] Calabrese P and Cardy J 2005 Evolution of entanglement entropy in one-dimensional systems *J. Stat. Mech.* 04010
[47] Calabrese P and Cardy J 2007 Entanglement and correlation functions following a local quench: a conformal field theory approach *J. Stat. Mech.* 10004
[48] Wen X and Wu J-Q 2018 Floquet conformal field theory (arXiv:1805.00031)
[49] Wen X, Fan R, Vishwanath A and Gu Y 2021 Periodically, quasiperiodically and randomly driven conformal field theories *Phys. Rev. Res.* **3** 023044
[50] Fan R, Gu Y, Vishwanath A and Wen X 2020 Emergent spatial structure and entanglement localization in floquet conformal field theory *Phys. Rev.* X **10** 031036
[51] Wen X and Wu J-Q 2018 Quantum dynamics in sine-square deformed conformal field theory: quench from uniform to nonuniform conformal field theory *Phys. Rev.* B **97** 184309
[52] Lapierre B, Choo K, Tauber C, Tiwari A, Neupert T and Chitra R 2020 Emergent black hole dynamics in critical Floquet systems *Phys. Rev. Res.* **2** 023085
[53] Fan R, Gu Y, Vishwanath A and Wen X 2021 Floquet conformal field theories with generally deformed Hamiltonians *SciPost Phys.* **10** 049
[54] Lapierre B and Moosavi P 2021 Geometric approach to inhomogeneous Floquet systems *Phys. Rev.* B **103** 224303
[55] Han B and Wen X 2020 Classification of S L_2 deformed Floquet conformal field theories *Phys. Rev.* B **102** 205125
[56] Lapierre B, Choo K, Tiwari A, Tauber C, Neupert T and Chitra R 2020 The fine structure of heating in a quasiperiodically driven critical quantum system (arXiv:2006.10054)
[57] Andersen M, Nørfjand F and Zinner N T 2020 The real-time correlation function of floquet conformal fields (arXiv:2011.08494)
[58] Ageev D S, Bagrov A A and Iliasov A A 2021 Deterministic chaos and fractal entropy scaling in Floquet conformal field theories *Phys. Rev.* B **103** L100302
[59] Das D, Ghosh R and Sengupta K 2021 Conformal Floquet dynamics with a continuous drive protocol *J. High Energy Phys.* JHEP05(2021)172
[60] Wen X, Gu Y, Vishwanath A and Fan R 2021 Periodically, quasi-periodically, and randomly driven conformal field theories (ii): Furstenberg's theorem and exceptions to heating phases (arXiv:2109.10923)
[61] Das S, Ezhuthachan B, Kundu A, Porey S, Roy B and Sengupta K 2022 Out-of-time-order correlators in driven conformal field theories *J. High Energy Phys.* JHEP08(2022)221
[62] Bermond B, Chernodub M, Grushin A G and Carpentier D 2022 Anomalous Luttinger equivalence between temperature and curved spacetime: from black hole's atmosphere to thermal quenches (arXiv:2206.08784)
[63] Choo K, Lapierre B, Kuhlenkamp C, Tiwari A, Neupert T and Chitra R 2022 Thermal and dissipative effects on the heating transition in a driven critical system (arXiv:2205.02869)
[64] Wen X, Fan R and Vishwanath A 2022 Floquet's refrigerator: conformal cooling in driven quantum critical systems (arXiv:2211.00040)
[65] Liu X, McDonald A, Numasawa T, Lian B and Ryu S 2023 Quantum quenches of conformal field theory with open boundary (arXiv:2309.04540)
[66] Nozaki M, Tamaoka K and Tian Tan M 2023 Inhomogeneous quenches as state preparation in two-dimensional conformal field theories (arXiv:2310.19376)
[67] Lapierre B, Numasawa T, Neupert T and Ryu S 2024 Floquet engineered inhomogeneous quantum chaos in critical systems (arXiv:2405.01642)
[68] Das D, Das S R, Kundu A and Sengupta K 2023 Exactly solvable floquet dynamics for conformal field theories in dimensions greater than two (arXiv:2311.13468)
[69] Goto K, Nozaki M, Ryu S, Tamaoka K and Tan M T 2024 Scrambling and recovery of quantum information in inhomogeneous quenches in two-dimensional conformal field theories *Phys. Rev. Res.* **6** 023001
[70] Malvimat V, Porey S and Roy B 2024 Krylov Complexity in $2d$ CFTs with $SL(2,\mathbb{R})$ deformed Hamiltonians (arXiv:2402.15835)
[71] Goto K, Guo T Nosaka T, Nozaki M, Ryu S and Tamaoka K 2024 Spatial deformation of many-body quantum chaotic systems and quantum information scrambling *Phys. Rev.* B **109** 054301
[72] Goto K, Nozaki M, Tamaoka K, Tian Tan M and Ryu S 2021 Non-equilibrating a black hole with inhomogeneous quantum quench (arXiv:2112.14388)

J. Stat. Mech. (2024) 103103

[73] Caputa P and Ge D 2023 Entanglement and geometry from subalgebras of the Virasoro algebra *J. High Energy Phys.* JHEP06(2023)159
[74] de Boer J, Godet V, Kastikainen J and Keski-Vakkuri E 2023 Quantum information geometry of driven CFTs *J. High Energy Phys.* JHEP09(2023)087
[75] Kudler-Flam J, Nozaki M, Numasawa T, Ryu S and Tian Tan M 2023 Bridging two quantum quench problems—local joining quantum quench and Möbius quench – and their holographic dual descriptions (arXiv:2309.04665)
[76] Bernamonti A, Galli F and Ge D 2024 Boundary-induced transitions in Möbius quenches of holographic BCFT (arXiv:2402.16555)
[77] Miyata A, Nozaki M, Tamaoka K and Watanabe M 2024 Hawking-Page and entanglement phase transition in 2d CFT on curved backgrounds (arXiv:2406.06121)
[78] Jiang H and Mezei M 2024 New horizons for inhomogeneous quenches and Floquet CFT (arXiv:2404.07884)
[79] Das S, Ezhuthachan B, Kundu A, Porey S, Baishali R and Sengupta K 2023 Brane detectors of a dynamical phase transition in a driven CFT *SciPost Phys.* **15** 202
[80] Das S, Ezhuthachan B, Porey S and Roy B 2024 Notes on heating phase dynamics in Floquet CFTs and Modular quantization (arXiv:2406.10899)
[81] Bisognano J J and Wichmann E H 1975 On the duality condition for a Hermitian scalar field *J. Math. Phys.* **16** 985
[82] Bisognano J J and Wichmann E H 1976 On the duality condition for quantum fields *J. Math. Phys.* **17** 303
[83] Casini H and Huerta M 2009 Reduced density matrix and internal dynamics for multicomponent regions *Class. Quantum Grav.* **26** 185005
[84] Mintchev M and Tonni E 2021 Modular Hamiltonians for the massless Dirac field in the presence of a boundary *J. High Energy Phys.* JHEP03(2021)204
[85] Fries P and Reyes I A 2019 Entanglement Spectrum of Chiral Fermions on the Torus *Phys. Rev. Lett.* **123** 211603
[86] Cardy J and Tonni E 2016 Entanglement Hamiltonians in two-dimensional conformal field theory *J. Stat. Mech.* 123103
[87] Ryu S and Hatsugai Y 2006 Entanglement entropy and the Berry phase in the solid state *Phys. Rev.* B **73** 245115
[88] Li H and Haldane F D M 2008 Entanglement spectrum as a generalization of entanglement entropy: identification of topological order in non-abelian fractional quantum hall effect states *Phys. Rev. Lett.* **101** 010504
[89] Pollmann F, Turner A M, Berg E and Oshikawa M 2010 Entanglement spectrum of a topological phase in one dimension *Phys. Rev.* B **81** 064439
[90] Qi X-L, Katsura H and Ludwig A W W 2012 General relationship between the entanglement spectrum and the edge state spectrum of topological quantum states *Phys. Rev. Lett.* **108** 196402
[91] Bauer B, Cincio L, Keller B P, Dolfi M, Vidal G and Trebst S *et al* 2014 Chiral spin liquid and emergent anyons in a Kagome lattice Mott insulator *Nat. Commun.* **5** 5137
[92] Miyaji M, Ryu S, Takayanagi T and Wen X 2015 Boundary states as holographic duals of trivial spacetimes *J. High Energy Phys.* JHEP05(2015)152
[93] Witten E 2018 Aps medal for exceptional achievement in research: invited article on entanglement properties of quantum field theory *Rev. Mod. Phys.* **90** 045003
[94] Casini H and Huerta M 2023 Lectures on entanglement in quantum field theory *Theoretical Advanced Study Institute 2021* p 2
[95] Affleck I and Ludwig A W W 1991 Universal noninteger "ground-state degeneracy" in critical quantum systems *Phys. Rev. Lett.* **67** 161
[96] Calabrese P and Cardy J 2016 Quantum quenches in 1 + 1 dimensional conformal field theories *J. Stat. Mech.* 064003
[97] Blöte H W J, Cardy J L and Nightingale M P 1986 Conformal invariance, the central charge and universal finite-size amplitudes at criticality *Phys. Rev. Lett.* **56** 742
[98] Wen X, Ryu S and Ludwig A W W 2018 Entanglement Hamiltonian evolution during thermalization in conformal field theory *J. Stat. Mech.* 113103
[99] Zhu W, Huang Z, He Y-C and Wen X 2020 Entanglement Hamiltonian of many-body dynamics in strongly correlated systems *Phys. Rev. Lett.* **124** 100605
[100] Cho G Y, Ludwig A W W and Ryu S 2017 Universal entanglement spectra of gapped one-dimensional field theories *Phys. Rev.* B **95** 115122
[101] Calabrese P and Cardy J 2009 Entanglement entropy and conformal field theory *J. Phys. A: Math. Gen.* **42** 504005

J. Stat. Mech. (2024) 103103

[102] Nozaki M, Numasawa T and Takayanagi T 2013 Holographic local quenches and entanglement density *J. High Energy Phys.* JHEP05(2013)080
[103] Nozaki M, Numasawa T and Takayanagi T 2014 Quantum entanglement of local operators in conformal field theories *Phys. Rev. Lett* **112** 111602
[104] He S, Numasawa T Takayanagi T and Watanabe K 2024 Quantum dimension as entanglement entropy in 2D CFTs (arXiv:1403.0702)
[105] Wen X, Chang P-Y and Ryu S 2015 Entanglement negativity after a local quantum quench in conformal field theories *Phys. Rev.* B **92** 075109
[106] Asplund C T and Bernamonti A 2014 Mutual information after a local quench in conformal field theory *Phys. Rev.* D **89** 066015
[107] Ugajin T 2013 Two dimensional quantum quenches and holography (arXiv:1311.2562)
[108] Mao W, Nozaki M, Tamaoka K and Tian Tan M 2024 Local operator quench induced by two-dimensional inhomogeneous and homogeneous CFT Hamiltonians (arXiv:2403.15851)
[109] Su L, Clerk A and Martin I 2024 Dynamics and phases of nonunitary Floquet transverse-field Ising model *Phys. Rev. Res.* **6** 013131
[110] Peschel I 2003 LETTER TO THE EDITOR: Calculation of reduced density matrices from correlation functions *J. Phys. A: Math. Gen.* **36** L205

J. Stat. Mech. (2024) 103103